POTENTIAL IMPACTS OF OCEAN ACIDIFICATION ON DIATOM AGGREGATION WHEN EXPOSED TO CRUDE OIL AND CHEMICAL DISPERSANTS

A Thesis

by

JENNIFER LYNNE GENZER

Submitted to the Office of Graduate and Professional Studies of
Texas A&M University
in partial fulfillment of the requirements for the degree of

MASTER OF SCIENCE

Chair of Committee,	Antonietta Quigg
Committee Members,	Peter Santschi
	Jason Sylvan
Head of Department,	Jaime Alvarado-Bremer

August 2019

Major Subject: Marine Biology

Copyright 2019 Jennifer Genzer

ABSTRACT

Ocean acidification (OA) and its effects on seawater carbonate chemistry will affect all marine organisms, especially those that utilize inorganic carbon for photosynthesis. Diatoms, a group of silicifying phytoplankton, play a key role in the marine carbon cycle due to their high primary productivity rates, worldwide distribution, and production of extracellular polymeric substances (EPS). These exudates lead to marine snow formation that rapidly transports organic material to the seafloor. Diatoms also produce EPS for protection from harmful substances, such as oil spills. The effects of oil compounds on phytoplankton in future OA conditions has not been well studied. Roller table experiments with *Thalassiosira pseudonana*, a small centric diatom, were conducted to produce marine snow aggregates in six treatments: Control (pCO_2 = 400 ppm), OA (pCO_2 = 750 ppm), water accommodated fraction of oil (WAF), OAWAF, diluted chemically enhanced WAF (DCEWAF), and OADCEWAF. Measurements included photophysiological responses, oil concentrations, aggregate morphology, and exudate production to investigate if OA will affect the response to oil spill conditions. Marine snow and marine oil snow (MOS) formed in all treatments, but to varying sizes and amounts. The WAF and DCEWAF treatments simulating two spill conditions induced varying responses from *T. pseudonana*. WAF and OAWAF aggregates had less total area and accumulated more PAHs from the surrounding seawater (SSW), but DCEWAF and OADCEWAF aggregates incorporated a higher relative amount of polycyclic aromatic hydrocarbons (PAHs) based on the initial concentrations. Additionally, transparent exopolymeric particles (TEP) and EPS production increased in presence of petroleum compounds. Larger aggregates formed in OA, OAWAF and OADCEWAF compared to their current day counterparts, subsequently capturing more cells and oil compounds. The cell accumulation within

aggregates was similar between the stationary and exponential growth phase experiments, but the pre-existing concentrations of exudates from the culture were what most likely affected the distinctive aggregate formations. Based on the aggregate area and morphology, it was determined that OA affected aggregate formations, and subsequently may affect the biological carbon pump. The findings of this study will inform first responders as they plan to address future oil spills.

ACKNOWLEDGEMENTS

My greatest thanks goes to my committee chair, Dr. Antonietta Quigg, for providing me with endless opportunities while pursuing my master's degree in her lab. You have helped me grow into the scientist and person I am today. Thank you for your never-ending support, advice, guidance, and patience, and for allowing me to be the goofy troublemaker in the lab. Thank you to my committee members, Dr. Peter Santschi and Dr. Jason Sylvan, for your time and dedication to supporting me throughout my thesis research.

Thank you to everyone in the Phytoplankton Dynamics Lab. You have become a family to me, and this work would not have been possible without your helpful hands. Thank you to my sister forever, Jessica Hillhouse, for helping with all aspects of my research and for going on so many great adventures with me. Thank you Rachel Windham for answering all my inane questions and helping me from my very first day as a research assistant to my last day as a graduate student. Additionally, thank you to so many lab members that I have had the pleasure of getting to know, from fellow graduate students (Allyson Lucchese, Samantha Setta, Alicia Williams), to undergraduates (Austin Perez and Andrew Mondragon), research assistants (Noah Clafflin and Amelia McAmis), and post-doctoral researchers (Jamie Steichen, Laura Bretherton, and Manoj Kamalanathan).

Thank you to my cats, Sophie and Mako, for always being there for cuddles and love. Thank you to my family and friends for the unfailing support and love you have provided me through my graduate school journey. Thank you Grandma for always believing in me. I love you all so very much.

NOMENCLATURE

AB	Alcian Blue
ASW	Artificial seawater
AGG	Aggregate slurry
CCM	Carbon concentrating mechanism
CEWAF	Chemically enhanced water accommodated fraction of oil
DCEWAF	Diluted chemically enhanced water accommodated fraction of oil
DI	Deionized water
DIC	Dissolved inorganic carbon
DCM	Dichloromethane
DwH	Deepwater Horizon
EPS	Extracellular polymeric substances
EOE	Estimated oil equivalent
ESD	Equivalent spherical diameter
FIRe	Fluorescence Induction and Relaxation
MOS	Marine oil snow

MOSSFA	Marine oil snow sedimentation and flocculent accumulation
OA	Ocean acidification
OADCEWAF	Dilute chemically enhanced water accommodated fraction of oil with enhanced pCO_2
OAWAF	Water accommodated fraction of oil with enhanced pCO_2
PAHs	Polycyclic aromatic hydrocarbons
pCO_2	Partial pressure of carbon dioxide
POC	Particulate organic carbon
PSII	Photosystem II
ρ	Connectivity factor of PSII
SSW	Surrounding seawater
σPSII	Photosynthetic antennae size
TA	Total alkalinity
TEP	Transparent exopolymer particles
WAF	Water accommodated fraction of oil
XS	Extra small

CONTRIBUTORS AND FUNDING SOURCES

Contributors

This work was supervised by a thesis committee consisting of Professor Antonietta Quigg, Professor Peter Santschi of the Department of Marine Science, and Professor Jason Sylvan of the Department of Oceanography.

This thesis benefitted from the help of many collaborators. Dr. Uta Passow and Julia Sweet processed the TEP samples, Dr. Terry Wade and Dr. Gopal Bera analyzed the PAH samples, and Dr. Kathleen Schwehr and Charles Bergen processed the EPS samples. All other work conducted for the thesis was completed by the student independently.

Funding Sources

Graduate study was supported by the Gulf of Mexico Research Initiative (GOMRI) funded consortium research entitled ADDOMEx (Aggregation and Degradation of Dispersants and Oil by Microbial Exopolymers) and ADDOMEx-2. Data are publicly available through the Gulf of Mexico Research Initiative Information and Data Cooperative (GRIIDC) at http://data.gulfresearchinitiative.org. One semester of funding was awarded as a graduate assistant teaching fellowship from Texas A&M University.

TABLE OF CONTENTS

Page

Page

LIST OF FIGURES

Page

Page

Page

LIST OF TABLES

Page

INTRODUCTION

1.1 Phytoplankton

Phytoplankton are found across all bodies of water, but are constrained to the euphotic zone where they can readily obtain the sunlight required for primary production. These microscopic algae are invisible to the naked eye, ranging from 2 to 2000 µm, but are responsible for 50%, or 50 Pg C per year, of total inorganic carbon fixation through photosynthesis (Finkel et al., 2009; Chavez et al., 2011). At the base of marine ecosystems, phytoplankton provide nutrients for higher trophic levels and are vital for marine biogeochemical cycling of carbon, nitrogen, phosphorous, and silicon. Phytoplankton are essential to the biological carbon pump due to their production and contribution of organic carbon that sinks through the water column as marine snow aggregates and provides valuable resources to heterotrophic organisms (Fischer and Karakas, 2009; Passow and Carlson, 2012; Basu et al., 2018). Phytoplankton exude extracellular polymeric substances (EPS) and transparent exopolymer particles (TEP) into the water in stress inducing environments, as a first response to toxic compounds, or during large bloom events (Passow et al., 1994; Passow, 2002; Quigg et al., 2016; Santschi, 2018; Schwehr et al., 2018). Studying this contribution of phytoplankton derived organic material can help illustrate the affects to organisms across the food web. Once these aggregates reach the deep ocean, either bacterial degradation releases inorganic carbon back into the system, or the particles become recalcitrant and are buried in sediments (Chisholm, 2000).

1.2 Ocean Acidification

Since the start of the Industrial Revolution, anthropogenic sourced carbon dioxide (CO_2) has been accumulating in the atmosphere due to human population growth, expansion, and technological development (Gattuso and Hansson, 2011). Over the last 250 years, 30% of the anthropogenic CO_2 has been absorbed into the ocean, resulting in a downward shift in seawater pH (Sabine et al., 2004; Khatiwala et al., 2013). Gaseous CO_2 has always buffered into ocean surface waters, but the rapid buildup is affecting the rate at which it dissolves. This sudden increase of dissolved inorganic carbon is causing changes in oceanic carbonate chemistry through a process called ocean acidification (OA) (Royal Society, 2005). When CO_2 is absorbed into oceanic surface waters, it increases the concentration of hydrogen ions by binding with water and carbonate ions (CO_3^{2-}). These newly formed bicarbonate ions (HCO_3^-) decrease oceanic pH and make carbonate ions less bioavailable for marine calcifying organisms (Yamamoto-Kawai et al., 2009). Before the Industrial Revolution, the ocean's pH was 8.2; it is projected to reach 7.9 by the end of this century (Caldeira and Wickett, 2003; Royal Society, 2005). To date, the pH of the surface ocean has dropped to 8.1, which on a logarithmic scale is a 25% change and will have long-term effects (NOAA, 2017).

Not only will the ocean continue to acidify, but climate change will also disrupt the biological carbon pump (Figure 1.1) due to its impacts to oceanic temperatures, stratification of the water column, nutrient availability and cycling, and ultimately phytoplankton community composition and primary productivity (Behrenfeld et al., 2006; Finkel et al., 2009; Seebah et al., 2014). Some species of phytoplankton, particularly within the Haptophytes, rely on the calcium carbonate present in the upper water column to form their shells. These phytoplankton, along with other calcifying organisms such as bivalves, coral, and fish otoliths, are those getting the most

attention in OA research (e.g., Beardall and Raven, 2013; Perry et al., 2015; Waldbusser et al., 2015). However, non-calcifying groups of phytoplankton are likely to be affected as well but are not as commonly studied in this field. Diatoms, which are responsible for about 40% of marine inorganic carbon fixation (Mann, 1999; Wu et al., 2014), and whose frustule silicification may be affected by OA (Milligan et al., 2004), have until recently been understudied. In addition to the potential impact of OA on diatoms, m any harmful algal bloom species (i.e. dinoflagellates) are likely to move into different regions with increasing temperatures and changing currents, resulting in blooms in new regions (Pedersen and Hansen, 2003; Barton et al., 2016). Studying a variety of marine life is important when considering the overall uncertainty of the physiological and ecological effects of changes to marine carbonate systems (McCarthy et al., 2012).

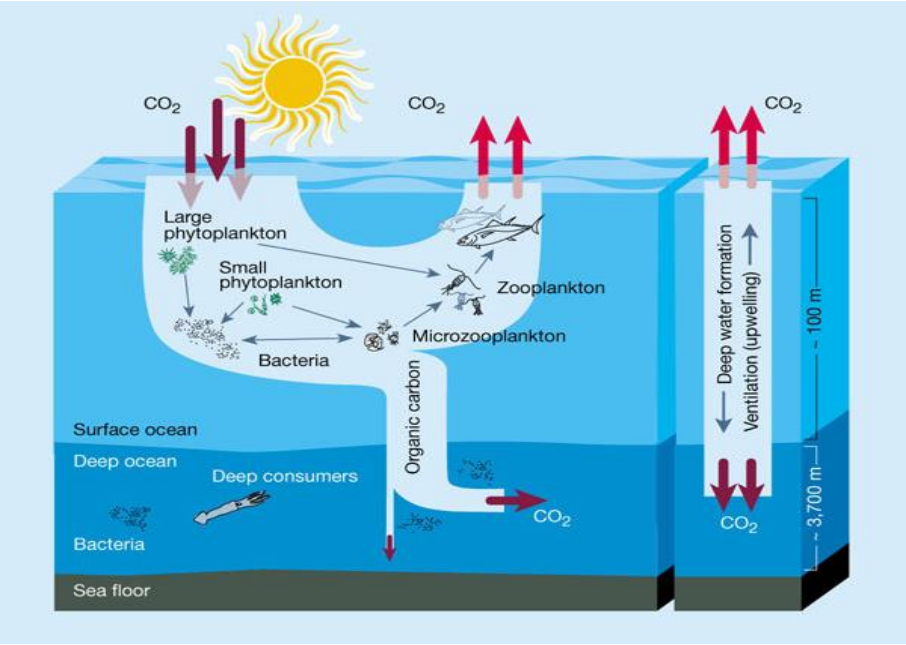

Figure 1.1 Diagram detailing the essential role of phytoplankton in the ocean's biological carbon pump due to their contribution of organic carbon through the water column (Chisholm, 2000). Reprinted by permission from Springer Nature: Nature 407, Stirring times in the Southern Ocean by Sallie W. Chisholm, 2000.

1.3 Deepwater Horizon oil spill

The Deepwater Horizon (DwH) blowout occurred on April 20, 2010 off the coast of Louisiana in the Gulf of Mexico. The disrupted wellhead continuously leaked crude oil and natural gas for 87 days until it was sealed on September 19, spilling an estimated 4.1 million barrels of crude Louisiana Sweet Oil and resulted in the largest marine oil spill in history (Crone and Tolstoy, 2010; Reddy et al., 2012). Most of the oil rose to the sea surface, due to its nonpolar properties, and created an oil slick. Responders used multiple methods of remediation, including skimming, burning, and applying chemical dispersant to limit the impact to coastal environments. An estimated 37,500 barrels of the dispersants, Corexit 9500A and Corexit 9527, were applied over the course of the spill at the exposed wellhead and sea surface, which was more than any previous spill (TFISG, 2010; Kujawinski et al., 2011). This chemical remediation has been debated ever since due to the potential environmental impact of increased oil concentrations in the water column and the broad scale use of the dispersant itself (Bælum et al., 2012).

In addition to human remediation efforts, there was natural degradation and transportation of the released oil. In the weeks following the DwH oil spill, there were region-wide sightings of large, fast sinking marine snow (Passow et al., 2012). Oil budget assessments suggest that up to 15% of the released oil was returned to the seafloor through these marine oil snow (MOS) aggregates in an event now called marine oil snow sedimentation and flocculent accumulation (MOSSFA) (Valentine et al., 2014; Daly et al., 2016; Passow and Hetland, 2016; Passow and Ziervogel, 2016; Quigg et al., 2019). Recently, MOSSFA has been under intense study because it significantly contributed to bioremediation and oil transportation following the DwH spill (e.g., Passow et al., 2012; Daly et al., 2016; Passow, 2016; Quigg et al., 2019). The biological mechanisms and activations of these events are not fully understood, however, it has been

documented that microbial exudates, like EPS and TEP, and oil-mineral aggregates were contributors (Khelifa et al., 2005; Passow et al., 2012). Organic matter like EPS and TEP are precursors composed of proteins and polysaccharides that can attract the nonpolar oil components and even envelop oil droplets. Oil-mineral aggregates are smaller than marine snow, < 50µm, but can contribute significantly to moving oil from the surface to the sea floor depending on wave conditions and the available material (Khelifa et al., 2005). OA may affect these bioremediation events if the biological carbon pump weakens and becomes less efficient at carbon transportation. Combining these two areas of study would not only contribute to both topics individually, but may also provide insight into how a future oil spill could affect the primary producers in coastal environments.

1.4 Thalassiosira pseudonana

Diatoms are silicifying phytoplankton that are an essential component of the marine carbon cycle because of they are responsible for 40% of the total marine global primary productivity every year (Mann, 1999). They are also well-documented EPS and TEP producers that enhance aggregation and contribute to marine snow transportation of nutrients and organic carbon to the seafloor (Thornton, 2002). Larger diatoms may be limited by OA and changing nutrient availability, potentially instigating a shift towards smaller species due to their high cell surface area to volume ratio, which allows for more efficient nutrient uptake (Bopp et al., 2005). *Thalassiosira pseudonana* is globally abundant diatom (Figure 1), that has been a model laboratory species since its genome was sequenced by Ambrust et al. (2004). Many laboratory studies have shown that *T. pseudonana* has no significant growth or photosynthetic response to OA conditions (Crawfurd et al., 2011; McCarthy et al., 2012; Yang and Gao, 2012; Wu et al., 2014). This may be

due to its small size, 2 to 10 µm, and high surface area to volume ratio that facilitates diffusion of CO_2 into the cell, and its use of carbon concentrating mechanisms (CCMs) which surrounds ribulose bisphosphate carboxylase-oxygenase, the carbon-fixing enzyme, with CO_2, pushing it towards carboxylation. Studies focusing on other phytoplankton species show CCMs operating within cells negate possible benefits of having more carbon dioxide available in OA conditions (Bach et al., 2011; Wu et al., 2014). Other studies have disagreed on the response of *T. pseudonana* prompted by OA conditions; these differing results may be caused by discrepancies between environmental setups and treatments tested (Shi et al., 2016; Yuan et al., 2018). Detailed experiments focusing on the effect of OA on small diatoms at the beginning and end of their role in the biological carbon pump may be beneficial for applying laboratory studies to a larger scale. The work presented here is unique because it investigated how OA affects marine snow production and aggregation in the presence of oil spill conditions at both the intracellular and extracellular level.

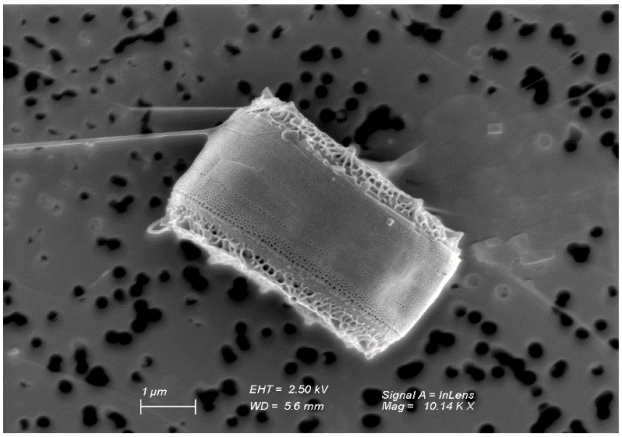

Figure 1.2 An image of Thalassiosira pseudonana *taken using a scanning electron microscope by Dr. Manoj Kamalanathan showing the cell shape and strings of exudate.*

STUDY AIM

In previous laboratory experiments, ten isolated culture strains of phytoplankton were screened for their growth rates, chlorophyll *a* content, photosynthetic efficiency and other photophysiological effects after being exposed to oil and chemically dispersed oil (Bretherton et al., 2018). *T. pseudonana* was one of the species identified as sensitive to all treatments with added petro-carbons. The current study delved further into *T. pseudonana*'s response to oil and dispersant and additionally incorporated present and future ocean conditions. Specifically, this study was designed to test the hypothesis that ocean acidification led to changes in exudate production, marine snow formation, and oil accumulation within aggregates by the diatom *Thalassiosira pseudonana* in response to an oil spill. To address that hypothesis, *T. pseudonana* was inoculated into six treatments: (i) Control (pCO_2 = 400 ppm), (ii) enhanced pCO_2 (pCO_2 = 750 ppm) (OA), (iii) water accommodated fraction of oil (WAF), (iv) WAF with enhanced pCO_2 (OAWAF), (v) diluted chemically enhanced WAF (DCEWAF), and (vi) DCEWAF with enhanced pCO_2 (OADCEWAF). *T. pseudonana* was maintained in either exponential or stationary growth phase before beginning each experiment to investigate any variation in between growth phases of the same species.

METHODS

3.1 Culturing and establishing carbonate conditions

Isolated *Thalassiosira pseudonana* (CCMP 1335) culture was obtained from the National Center for Marine Algae and maintained long term in natural seawater enriched with f/2 + Si nutrients (Guillard and Ryther, 1962; Guillard, 1975). The seawater was retrieved from the NOAA National Marine Fisheries Services in 20 L carboys, brought to Texas A&M University at Galveston, and filtered with a Millipore disposable 0.45 µm ground filter to remove particulates. The seawater was stored refrigerated until ready for use. The filtered seawater was autoclaved to 120ºC to sterilize, and f/2 nutrients were added once cooled to eliminate loss through precipitation in the heated water. For the stationary growth phase experiment, the culture was maintained and bulked in this natural seawater media.

One month prior to the exponential growth phase experiment, 200 mL of *T. pseudonana* culture grown in natural seawater enriched with f/2 + Si nutrients was transferred into artificial seawater (ASW) with f/2 + Si nutrients. From there, the culture was continuously maintained in exponential growth phase with regular dilutions of this nutrient enriched ASW. The artificial seawater was prepared according to Berges et al. (2001) with a few modifications. The deionized (DI) water used to make the artificial seawater was not sterilized because it permanently alters the carbonate system (Seebah et al., 2014). The artificial seawater anhydrous and hydrated salts need to be added as two separate solutions to keep them from interacting and not properly dissolving. The two salts were therefore prepared separately and spun on a stir plate for an hour before they were combined (Table A1). Then they were allowed to spin for another hour before the salinity was checked and f/2 + Si nutrients were added. The pH was adjusted by adding small quantities

of Trizma base to bring the pH to 8.1 before storing the media in a cold, dark room to reduce bacterial growth. The abundance of pre-existing TEP and EPS in natural seawater was avoided by using artificial seawater, which also reduced differences in starting seawater between experiments.

The cultures transferred into artificial seawater were maintained in exponential growth phase and grown in 1 L glass bottles at 19 ± 1°C under a 12h : 12h light : dark cycle and light intensity of 100-130 µmol m^{-2} s^{-1}. Culture cell densities were maintained below 300,000 cells mL^{-1} in exponentially growing cultures to prevent nutrient and light limitation. Cultures were transferred regularly to fresh media in order to keep them in exponential phase growth. Previous studies have found the precursor concentrations and the aggregation response of diatoms is dependent on the growth phase (Smetacek, 1985; Passow et al., 1994; Passow, 2002), so two sets of roller table experiments were performed: (a) using stationary growth phase cultures and (b) using exponentially growth phase cultures.

Three days prior to starting a roller table experiment, cultures were spilt into two groups: current day 400 ppm (Control), and enhanced pCO_2 to 750 ppm (OA). This adjustment period ensured that the enhanced pCO_2 level did not shock the culture, even though previous long-term studies have shown that this pCO_2 level may not have a significant effect on *T. pseudonana* (Crawfurd et al., 2011). The cultures were kept in triplicate 1 L bottles with no headspace. The pH was maintained at 8.1 for Control and 7.9 for OA cultures using acid and bicarbonate additions in 1 M solutions (Gattuso and Lavigne, 2009). The open access Seacarb R package (version 3.1.1) was used for calculating seawater chemical perturbations to reach these pCO_2 levels using salinity, temperature, pH, and total alkalinity (TA) (https://CRAN.R-project.org/package=seacarb). Salinity was measured using a refractometer, and along with temperature, remained consistent throughout the pCO_2 adjustment period. The initial pH was measured for each culture bottle using

an Accumet AB15 pH meter, which was calibrated daily to pH 4, 7, and 10. TA was determined using the pH meter and Equation 1. An aliquot of 100 mL (vol_{sample}) was poured into a beaker and incremental additions (vol_{acid}) of 1 M HCl (N_{acid}) were added to reach pH 4.5 (1). These values were input to the flag 8 argument in the Seacarb R script, along with temperature, total phosphates and silicates in the media, and the target pCO_2 level. The calculated chemical adjustment was given in mol kg^{-1} and was converted to mL L^{-1} for inoculation dosages. The determined acid and bicarbonate volumes for each bottle were then added to the culturing bottles, which were immediately sealed and placed back in the culturing room. These chemical perturbations were conducted daily at the same time prior to the experiments.

$$\text{Total alkalinity } (\mu\text{mol kg}^{-1}) = \left[\frac{vol_{acid} * N_{acid}}{vol_{sample}}\right] * 1{,}000{,}000 \quad (1)$$

3.2 Oil and dispersant treatments

Preparation of the large volume of WAF required a baffled recirculating tank to mix the oil and seawater (Figure 3.1). This system, built from non-tempered glass and silicon glue, utilized a continuous flow-through via recirculation pumps (Wade et al., 2017). The tank was filled with 120 L of artificial seawater with f/2 + Si nutrients, prepared as described above in 3.1, and treated with 48 mL of crude Macondo surrogate oil (0.4 mL of oil L^{-1} seawater) (Figure 3.1). An Arrow 1750 stirrer with a stainless steel rod and propeller was placed in one end of the tank and stirred at the third speed setting for 24 hours in the dark. An output and input hose was attached to a pump and inserted to both ends of the tank to circulate the water through the system continuously. This

pump system was also used to move WAF directly from the baffled recirculating tank into the roller tanks without disrupting the oil slick at the surface.

The second oil treatment incorporated Corexit, a chemical surfactant used for remediation following DwH (The chaos of clean up (TCCP), 2011). Following a modified protocol by the Chemical Response to Oil Spills: Ecological Research Forum (Aurand and Coelho, 2005; Wade et al., 2017), artificial seawater with f/2 nutrients was added to a 9 L glass aspirator instead of using the baffled recirculating tank. Again, 0.4 mL of oil L^{-1} seawater was added, but with the addition of Corexit in a 1:20 dilution. A stir bar was placed within the aspirator, and mixed the solution for 24 hours in the dark to make a chemically enhanced water accommodated fraction of oil (CEWAF). This method produces CEWAF heavily concentrated with oil (167.42 mg L^{-1}), which has been shown incapacitate *T. pseudonana* (Bretherton et al., 2018). Subsequently, it was diluted (DCEWAF) to match the estimated oil equivalent (EOE) measurements in the WAF (Methods 3.4). WAF and DCEWAF each had an enhanced pCO_2 counterpart (OAWAF and OADCEWAF respectively) to simulate an oil spill in future carbonate conditions.

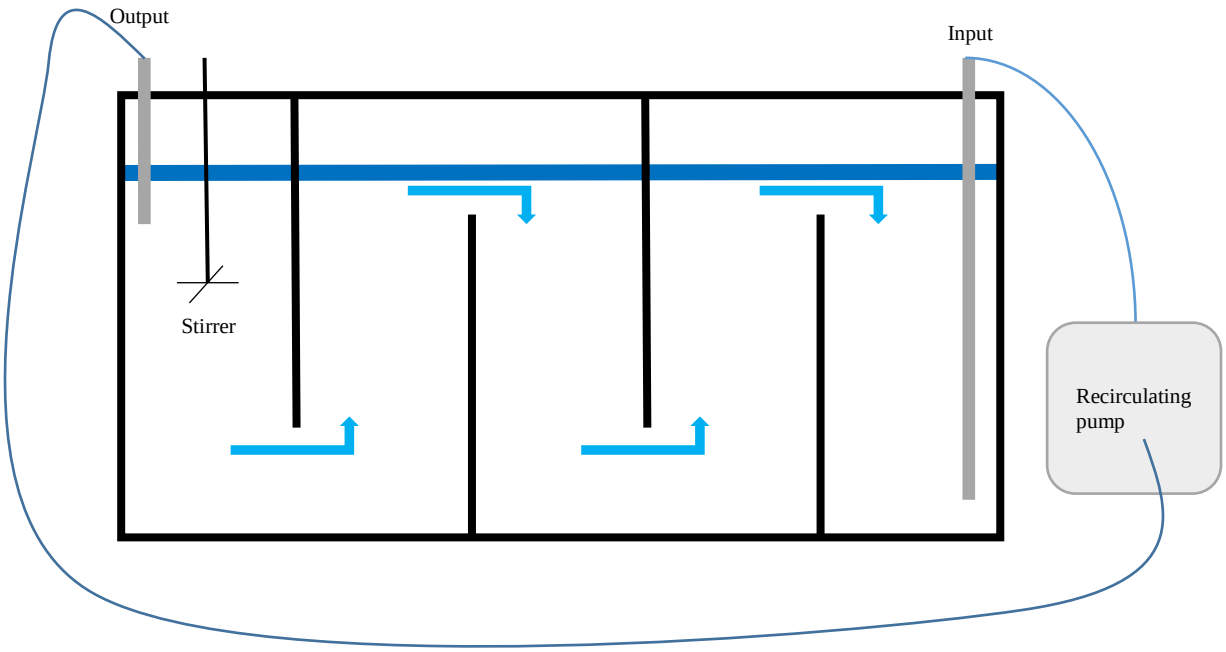

Figure 3.1 Diagram detailing how water flows through the baffled recircling tank system. A stirrer is shown on the left end, and a recirculating pump is connected on both ends.

3.3 Roller tanks and experimental design

The effects of ocean acidification and oil treatments on *T. pseudonana* marine snow formations were tested using cylindrical glass tanks placed on two rotating parallel bars (Figure 3.2). These roller tanks were continuously rolled to simulate sinking through the water column, and to allow organic particles to interact, coagulate, and form marine snow aggregates in a laboratory (Ploug et al., 2010; Passow and Carlson, 2012; Seebah et al., 2014; Passow, 2016). The motors that control the parallel bar rotations were set to roll the tanks 3 times per minute, which allowed aggregates to form and stay suspended in the tanks with minimal vertical travel within the system (Figure 3.2). The experiment was performed in total darkness to simulate deep ocean conditions and to reduce the effects of growth and primary productivity. The room temperature

was maintained at 19 ± 3°C to keep consistent with culture growth conditions. The experiments were run in separate batches due to logistical limitations, but the external experimental conditions remained consistent.

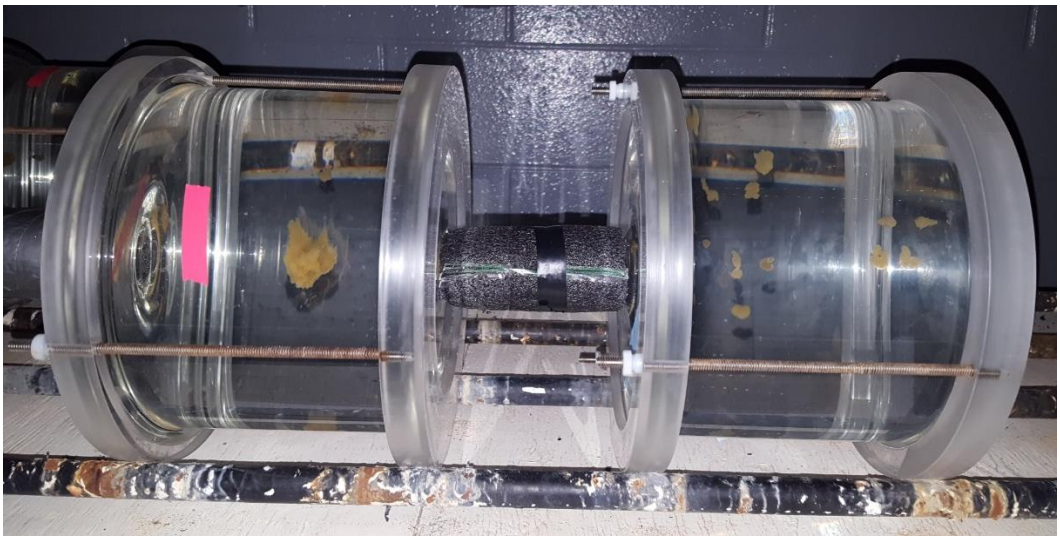

Figure 3.2 Roller tanks allow aggregates to form in different treatment conditions. The foam wrapped around the neck of the tanks kept them from colliding.

Prior to each experiment, all glassware, i.e. WAF making equipment, roller tanks and culture bottles, was triple rinsed with DI water, sterilized with 10% HCl for 24 hours, rinsed again with DI, and left to completely dry. Equipment that was exposed to oil was additionally triple rinsed sequentially with DCM, methanol and DI to remove residual petroleum compounds from the glassware. Roller tank labelling remained consistent between experiments so that the replicates A-C and those that were the pCO_2 enhanced did not vary. Tanks were broken down and cleaned individually to ensure no parts were switched between systems or pCO_2 conditions. Each was tested for O-ring leaks before each experiment by re-assembling and filling with DI. This process

of checking for leaks and using consistent stands, O-rings, tanks, lids and stoppers was utilized following the stationary growth phase experiment where some replicates were lost.

The two oil treatments, WAF and DCEWAF, were started 24 hours before each experiment. The morning of each experiment, *T. pseudonana* cultures were combined into two culture stocks, based on pCO_2 levels, for uniform cell and exudate additions to the roller tanks. The stocks were gently mixed, and an aliquot (1 mL) of each was preserved with 10% Lugols solution to perform cell counts with a hemocytometer in triplicate. The hemocytometer was filled with 10 µL on both sides of the slide, and the cells within the eight sections were counted. This process was done in triplicate for both culture stocks, and the counts were averaged to calculate the *T. pseudonana* cells mL^{-1}. These counts were used to determine the volume of *T. pseudonana* necessary to reach a final cell density of 10,000 cells mL^{-1} in each tank.

The roller tanks were then filled through the neck using funnels and graduated cylinders; the inoculation volumes are shown in Table 3.1 for the two experiments. Air bubbles create turbulence within the system and disrupts aggregate formation, so these were minimized by slowly topping off the tanks and delicately maneuvering and rotating to allow bubbles to escape through the neck. Immediately before closing the tanks with the stopper, the chemical perturbations of acid and bicarbonate were added to reach desired OA conditions as described above (Gattuso and Lavigne, 2009). The roller tanks established the closed system necessary to eliminate air exchange that would disrupt the established pCO_2 conditions (Gattuso and Lavigne, 2009; Seebah et al., 2014). Bicarbonate was added before the acid to reduce alkalinity changes (Gattuso and Lavigne, 2009). The tanks were placed on the parallel bars with foam on the necks to protect them from slowly migrating into each other (Figure 3.2). An identical tank was prepared for each treatment, but was used for initial time point measurements instead. The rolling tanks were then left to

incubate in the dark to reduce biological activity with minimal interaction. Twice daily observations for aggregate formations and confirmation that the motors were operating were conducted with as little light introduction as possible. The first sightings of aggregate formations were recorded for all treatments.

After the three-day incubation, the tanks were processed individually by first carefully removing them from the rolling bars and placing them gently on their side (Figure 3.3). The total time (0-3 minutes) it took the aggregates to settle on the bottom of the tank was recorded for a settling time proxy in the exponential growth phase experiment. Disassembly began with removing the stopper and inserting one end of a Teflon tube into the neck of the tank. Each tank was then separated into the surrounding seawater (SSW) and aggregate slurry (AGG). A disposable plastic syringe was attached on the other end of the tube and used to create a pressure vacuum that gently removed the top water without disrupting the settled aggregates. This initial extracted volume was used to rinse the Teflon tube (50 mL) and SSW sample container (50 mL), or for particulate organic carbon (POC) and dissolved inorganic carbon (DIC) measurements (200 mL). The first 50 mL through the Teflon tube was disposed into a waste container, and the next 50 mL was used to triple rinse the SSW 6 L carboy. The third 50 mL removed was filtered onto a pre-combusted 0.7 µm GF/F filter (47 mm diameter) using a 1 L Nalgene filter tower and a GAST vacuum pump. The filtrate was used to rinse the tower and a pre-combusted amber glass bottle. Then, another 150 mL was removed from the roller tank and passed through the same filter. The filter was stored in a plastic tray and immediately frozen at -20ºC for POC and CHN analysis. The filtrate was poured into the amber bottle for DIC measurements and stored at 4ºC with the lid wrapped in parafilm and no remaining headspace. These initial measurements and rinses were necessary to remove enough water volume to dismantle the tank's lid.

Once the lids were removed, photographs of the aggregates were taken for size and count analysis (Figure 3.3). The disassembly table was lined with laminated 0.5 x 0.5 cm gridline paper in the stationary and 0.6 x 0.6 cm paper in the exponential growth phase experiment. The gridline paper was necessary for later size analysis using the ImageJ program to compare aggregate counts, shapes, and area (Methods 3.6) between treatments. Then, the Teflon tube and vacuum inducing syringe method was continued to transport SSW from the tank into the sample container until there was 3 inches of water remaining in the tank. An Eppendorf Combitip advanced syringe was used to remove and combine all aggregate material into a pre-weighed 50 mL vial. This AGG slurry was dense with cells and extracellular components and homogenized aggregate measurements within a tank. The two water fractions, AGG and SSW, were then brought back to the lab for immediate processing before continuing to the next tank. All replicates were processed before moving to the next treatment.

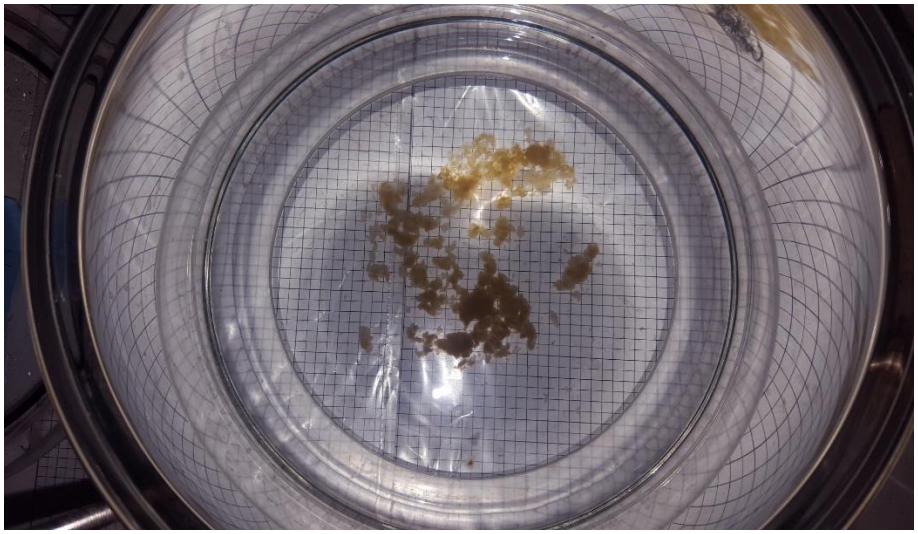

Figure 3.3 Representative photograph of a partially disassembled tank for ImageJ analysis before separating the aggregates from the surrounding seawater.

3.4 Oil analysis

Oil analysis was performed in two ways. Samples from each treatment (15 mL) were mixed with dichloromethane (DCM) (5 mL) to extract the nonpolar oil components from the sample. The DCM extraction was placed in quartz cuvettes and run on a RF-5301 PC Spectrofluorophotometer at 322 nm excitation and 376 nm emission wavelengths. A calibration curve was prepared using Macondo surrogate standard oil to determine the EOE (Wade et al., 2017). This was primarily used to confirm the concentrations in the roller tanks, and to match the concentrations between WAF and DCEWAF.

The EOE analysis showed an undetectable amount of oil in the Control and OA treatments for both the stationary and exponential growth phase experiments (Table 3.1). For the stationary phase experiment, the beginning concentrations were heterogeneous between WAF and OAWAF treatments, but the final oil concentrations were both measured at 0.12 mg L^{-1} in WAF and OAWAF treatments (Table 3.1). In the exponential growth phase experiment, the beginning EOE concentrations were similar between the oil treatments and ranged between 0.2 to 0.26 mg L^{-1} in WAF, OAWAF, DCEWAF and OADCEWAF treatments (Table 3.1).

Table 3.1 Descriptions of the treatments used in the stationary and exponential growth phase experiments. Initial and final EOE measurements (mg L^{-1}) are included for the treatments used in either study. Treatments not included in the stationary growth phase experiment denoted as not applicable (n/a).

	Treatment	Control	Enhanced pCO_2	Water accommodated fraction of oil	Water accommodated fraction of oil with enhanced pCO_2	Dilute chemically enhanced water accommodated fraction of oil	Dilute chemically enhanced water accommodated fraction of oil with enhanced pCO_2
	Abbreviation	Control	OA	WAF	OAWAF	DCEWAF	OADCEWAF
Stationary growth phase	Inoculation volumes	5.3 L ASW 0.4 L culture	5.3 L ASW 0.4 L culture	5.3 L WAF 0.4 L culture	5.3 L WAF 0.4 L culture	n/a	n/a
	Initial EOE	0	0	0.74 (± 0.02)	0.49 (± 0.05)	n/a	n/a
	Final EOE	0	0	0.12 (± 0.02)	0.12 (± 0.03)	n/a	n/a
Exponential growth phase	Inoculation volumes	5.3 L ASW 0.351 L culture	5.3 L ASW 0.32 L culture	5.4 L WAF 0.27 L culture	5.3 L WAF 0.32 L culture	5.2 L ASW 0.001 L CEWAF 0.45 L culture	5.2 L ASW 0.001 L CEWAF 0.43 L culture
	Initial EOE	0	0	0.26	0.2	0.2	0.2
	Final EOE	0	0	0.13 (± 0.01)	0.11 (± 0.01)	0.18 (± 0.12)	0.08 (± 0.02)

The second analysis was necessary for quantitative measurements of oil components at the beginning and end of the experiments. For each tank, samples of SSW (700 mL) and AGG (3 mL) was stored at -20°C in glass bottles until analysis for polycyclic aromatic hydrocarbons (PAHs). Prior to extraction, each sample was thawed to room temperature and spiked with 50 µL of internal standards (d_8-naphthalene, d_{10}-acenaphthene, d_{10}-phenanthrene, d_{12}-chrysene and d_{12}-perylene).

SSW samples were extracted with DCM by adding 50 mL to the bottles and shaking vigorously for 1 minute. The entire sample, both seawater and DCM, was poured into a glass 1 L separatory funnel. The sample bottle was rinsed with 25 mL of DCM, shaken, and poured into the funnel to limit loss. The separatory funnel was capped with a glass plug, and gently shaken for 1 minute while periodically pausing to release pressure buildup. It was placed on a rack and allowed to settle into the DCM and water fractions. After the two fractions were clearly settled and defined, the bottom DCM extracted layer was released into a 100 mL round bottom flask. This flask was set aside and covered with tin foil until all other samples were extracted. Separatory funnels were rinsed with DI water and DCM between replicates, and different funnels were used for each of the six treatments. AGG samples were processed differently than the SSW. First, each sample was placed in a 50 mL glass amber vial and extracted with 5 mL of DCM. After the DCM and water fractions formed clear separations, the DCM layer was transferred and passed through a Monstr-Pipette containing 1.0 g Silica Gel and 0.5 g Sodium Sulfate to remove the organic particulates that may interfere with later analysis. This separation column was rinsed with 3 mL of DCM to limit sample loss, and replaced after every sample. The extraction was stored in 25 mL glass vials covered with tin foil until analysis. They were then evaporated down, and spiked with recovery standards before being processed on a GC/MS (Wade et al., 2011; Morales-McDevitt et al., 2019).

3.5 Carbonate chemistry analysis

The marine carbonate status of a system can be determined using DIC, pCO_2, TA and pH measurements; having at least two of these is required to ensure acidified conditions reach desired values (Seebah et al., 2014). Several parameters of the seawater carbonate chemistry were measured in order to determine the established pCO_2 levels. Originally, DIC measurements were

going to be analyzed following Weisburd et al. (1995), but the results were interrupted by the presence of hydrocarbons. Instead, carbonate chemistry within the roller tank was determined following the protocols described in Methods 3.1 for pH, TA, and salinity, and the CO2SYS program built in Microsoft Excel (Pierrot et al., 2006) and the Seacarb R script were used for calculations.

For the stationary growth phase experiment, all treatments were below target pCO_2 levels (Table 3.2). The target pCO_2 for the controls was 400 ppm while the value calculated was 328 ppm. Similarly, the target pCO_2 for the OA treatments was 750 ppm while the value calculated was lower for OA and OAWAF (643 ppm and 695 ppm, respectively) (Table 3.2).

Table 3.2 Initial carbonate chemistry of each treatment in the stationary growth phase experiment. Calculations shown are from both CO2SYS and Seacarb R for pCO_2 *(ppm),* TCO_2 *(µmol kg* SW^{-1}*),* HCO_3^- *(µmol kg* SW^{-1}*),* CO_3^{2-} *(µmol kg* SW^{-1}*), and* CO_2 *(µmol kg* SW^{-1}*).*

	Measurement	Control	OA	WAF	OAWAF
Target	pH	8.1	7.9	8.1	7.9
	pCO_2	400	750	400	750
Measured	pH	8.15	7.9	8.15	7.87
	TA	2420	2420	2420	2420
CO2SYS	pCO_2	328	643	327	695
	TCO_2	2119	2246	2119	2259
	HCO_3	1895	2092	1895	2111
	CO_3	213	132	213	124
	CO_2	11	21	11	23
Seacarb R	pCO_2	327	643	327	695

The pCO_2 calculations showed that the target values of 400 and 750 ppm were not reached for the exponential growth phase experiment (Table 3.3). However, the pCO_2 levels between ambient and future conditions were significantly different from each other, and shifts were observed in pH.

Table 3.3 Initial carbonate chemistry of each treatment in the exponential growth phase experiment. Calculations shown are from both CO2SYS and Seacarb R for pCO_2 *(ppm),* TCO_2 *(µmol kg* SW^{-1}*),* HCO_3^- *(µmol kg* SW^{-1}*),* CO_3^{2-} *(µmol kg* SW^{-1}*), and* CO_2 *(µmol kg* SW^{-1}*).*

	Measurement	Control	OA	WAF	OAWAF	DCEWAF	OADCEWAF
Target	pH	8.1	7.9	8.1	7.9	8.1	7.9
	pCO_2	400	750	400	750	400	750
Measured	pH	8.1	7.9	8.1	7.9	8.17	7.99
	TA	2450	2450	2420	2420	2485	2485
CO2SYS	pCO_2	381	651	376	643	318	521
	TCO_2	2175	2275	2148	2246	2167	2266
	HCO_3	1965	2118	1940	2092	1928	2086
	CO_3	197	134	195	132	227	162
	CO_2	12	22	1	21	10	17
Seacarb R	pCO_2	381	651	376	643	318	521

3.6 Image analysis of the aggregates

The photographs taken of each tank during take down were manually processed using ImageJ software (Version 1.51j8). They were first converted to greyscale and calibrated to the gridline paper placed under the tank. Each of the 2,297 individual aggregates was outlined using the Polygon Selections tool at 400-x magnification, and the program measured the area, aspect

ratio, grey scale color density, perimeter, length and width, and more for a detailed view of aggregate morphology. The greyscale-converted image was compared to a full color version while analyzing to ensure shadows caused by the camera flash were not inadvertently included. The processed images (Figure 3.4) were saved to refer to during analysis.

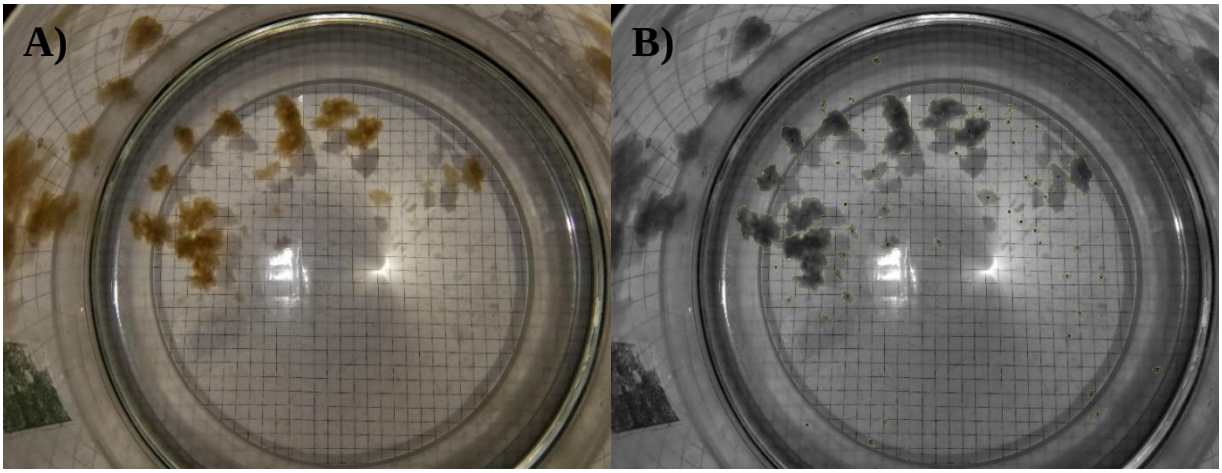

Figure 3.4 Raw photographs of each tank (A) were processed (B) using ImageJ analysis.

ImageJ aggregate area measurements from the exponential growth phase experiment were input into RStudio (Version 0.99.903) to create an agglomerative dendrogram with limited bias for size classes (Figure A6). Built-in packages were used for the Ward Hierarchical Clustering and the Euclidean method. Cutting the dendrogram tree at different heights partitions aggregates at that level, and less variability within a cluster is present when the height approaches zero. A small change in height does not add much power to warrant the addition of another size class, but a large leap adds distinction within the branching. Seen in Figure A6, the first cut occurred at 350 height and included large variability between the two branches. The second cutting dropped the height to

125, meaning the variability within the classes dropped substantially. The introduction of a fourth branch again lowered the height considerably, but the difference between four and five branches did not meaningfully drop the height. Both sets of clusters were analyzed, and it was determined that the addition of a fifth size class was unnecessary to the study because the branching occurred within the smallest aggregate size range. Therefore, the analysis moved forward with four size classes: Large (>4.683 cm^2), Medium (1.551 to 4.682 cm^2), Small (0.591 to 1.550 cm^2), and Extra Small (XS) (<0.590 cm^2). These area size classes were applied to the stationary and exponential phase experiments aggregates. Size classes can be built by setting numerical boundaries, such as doubling the range as the classes' increase, but this created too many classes to compare. This also made XS flake aggregates seem more of the focus to the study rather than the differences between the larger formations. Particles less than 0.5 mm were not included in this analysis because MOS is defined by this boundary (Quigg et al. 2016; Passow et al., 2017).

The ImageJ program also gave other defining measurements for each aggregate apart from area. The mean gray value was calculated within the program by averaging all the grey value's optical units within an aggregate, and was used in this study as a qualitative proxy for density. A few heat plots were generated within ImageJ in order to visualize this measurement, but were not quantitatively used (Figure A3). The closer the mean gray value on the optical unit scale was to zero, the darker the average pixel within that selection. The aspect ratio of each aggregate was used to measure elongation, and was defined as the major axis divided by the minor axis of the best fitting ellipse. Other measurements given by the program, such as the length of the perimeter, minimum and maximum gray value, width and height of the bounding rectangle, and roundness of each aggregate, were not included in this analysis.

Equivalent spherical diameter (ESD) measurements are commonly used in marine snow studies to normalize the aggregate sizes and shapes (Seebah et al., 2014; Daly et al., 2016; Passow, 2016; Passow et al., 2019) and sinking velocity (Passow et al., 2014). ESD has previously been measured using microscopes and grid paper to calculate the bio-volume by assuming an ellipsoid shape with the length, width and height measurements. In these experiments, the aggregates were not individually studied or measured for sinking, but immediately incorporated into an aggregate slurry. Instead, the ESD of each aggregate was calculated (Equation 2) using its ImageJ area (Williamson et al., 2003).

$$\text{Equivalent spherical diameter (cm)} = 2 * \sqrt{\left(\frac{\text{area}}{\pi}\right)} \quad (2)$$

This equation incorporates the area of an aggregate, fits the area to a perfect sphere, and calculates the diameter. The ESD was then converted from cm to mm and input into a previous study's sinking velocity (Equation 3) to determine the rate the aggregates would sink by the end of the experiment (Passow et al., 2019).

$$\text{Sinking velocity (m d}^{-1}) = 211*(\text{ESD}^{0.69}) \quad (3)$$

3.7 Photophysiology and photosynthetic efficiency

Chlorophyll *a* was measured following the EPA Method 445 (Arar and Collins, 1997). Both SSW and AGG samples were filtered onto 0.7 µm GF/F glass microfiber filters to color. The

filters were stored at -20°C in microcentrifuge tubes. To extract the pigment from the filters, each was unfolded, placed into a glass test tube with 5 mL of 40:60 solution of dimethyl sulfoxide (DMSO) to 90% acetone, and stored in the dark at 4°C. After 24 h, the filters were discarded and the extracted chlorophyll *a* was measured using a benchtop 10AU Turner Designs fluorometer. Chlorophyll concentrations were determined using Sigma chlorophyll to prepare a standard curve.

Initial cell counts showed that the experiment began with an average of 12,500 cells mL^{-1}. Final SSW cell counts using a hemocytometer were below detection limit and consequently removed from the analysis for the stationary experiment. The method changed for the exponential experiment to using a Beckman Coulter Counter to circumvent these limitations. Instead, chlorophyll *a* content was used for a biomass proxy.

Chlorophyll fluorescence measurements at the beginning and end of each experiment quantified changes in photosystem efficiency and photophysiology. A 5 mL aliquot of SSW was dark acclimated for 15 minutes before measured in the Satlantic Fluorescence Induction and Relaxation (FIRe) fluorometer for the minimum ($F_{o\ (ST)}$) and maximum ($F_{m(ST)}$) fluorescence values from the single turnover (ST) component of the induction curve (Kolber et al., 1998; Kromkamp and Forster, 2003). All samples were corrected with a filtered seawater blank to account for interference. Variable fluorescence (F_v) was calculated as the difference between $F_{o\ (ST)}$ and $F_{m(ST)}$. The quantum yield of photochemistry, which is a proxy for the phytoplankton photosystem efficiency, was determined as $F_v/F_m = (F_{o\ (ST)} - F_{m(ST)})/F_{m(ST)}$. Additionally, the functional absorption cross section of Photosystem II (PSII) and changes in photosynthetic antennae size (σPSII) and connectivity factor of PSII (ρ) were measured in the FIRe.

3.8 Extracellular materials

Exudates were measured in the exponential growth phase experiment with an acid polysaccharide staining technique and a quantifiable extraction method for proteins, neutral sugars, and uronic acids. TEP filtering (900 mL) occurred at the beginning and end of each experiment, with the exception of the DCEWAF treatments because Corexit interferes with this measurement (Passow et al., 2017). The total volume of Alcian Blue (AB) staining solution required for the experiment was filtered through a 0.2 µm syringe filter to ensure that the solution was clump-free. SSW was filtered through a 0.4 µm Isopore Membrane Filter in triplicate, stained with 0.5 mL AB solution (Passow and Alldredge, 1995), and stored at -20°C. Blanks of 0.5 mL AB were filtered for every sampling day. Later, all filters were shipped to the University of California at Santa Barbara for processing. First, the filters were unfolded and extracted in 80% H_2SO_4 for 2 h, then removed and discarded. The solvent with the extracted fraction was measured at 787 nm on a Genesys 10S UV-Vis spectrophotometer. The readings were compared to the AB blanks, and a calibrated with a Gum Xanthum (Gxan) equivalents curve.

Total carbohydrate and protein content was measured in both the AGG (0.5 mL subsample) and SSW (200 mL) at the end of the experiment. The samples were individually filtered using ultra-centrifugal membranes (3 kDa) in small increments to collect the colloidal fraction of SSW and the particulate of the AGG. The collected material was then triple rinsed with 18 MΩ –cm Milli-Q Type I water, and concentrated to 2 mL. This filtered fraction was used for neutral sugar, uronic acid, and protein measurements. The neutral sugar concentrations were measured with a glucose standard following the anthrone method (Morris, 1948), the uronic acids with a glucuronic acid (Sigma, CAS 6556-12-3) standard (Hung and Santschi, 2001), and the proteins with a Bovine Serum Albumin (BSA) (ThermoFisher, Pierce protein assay kit) standard following a modified

bicinchoninic acid method by Smith (1985) (Schwehr et al., 2018). The three measurements from these methods were then calculated to represent the organic carbon content, expressed as their standard equivalents. Then, the uronic acids and neutral sugars were combined for total carbohydrate content. The ratio of proteins/total carbohydrates in organic carbon equivalents was used for the stickiness of the colloidal EPS in SSW and the particulates in AGG.

3.9 Other analyses

The main organic measurements from this study are displayed in Table 3.4 for a brief overview on size fraction, description, and the methods used. In the stationary growth phase experiment, SSW (50 mL) was filtered following the POC methods described in Methods 3.3. However, instead of freezing the filters for POC analysis, these filters were placed in an oven at 40ºC for 72 h to remove the water. The filters were weighed on a mass balance scale, and the initial weight of the filter was subtracted to give the dry weight of the organic matter trapped on the filter.

In the exponential growth phase experiment, SSW was filtered for POC following the methods described in 3.3, along with 0.5 mL of the aggregate slurry. Filters were moved from the freezer into a drying oven for 24 h at 40ºC. They were then moved to a glass desiccator with 50 mL of 3 M HCl to remove inorganic carbon from the filters. The filters were then cut in half to eliminate blockages because the filters used were too large to pass through the instrument. They were then weighed and carefully packed in 5 x 9 mm tin caps. A calibration curve was made using the same tin caps and acetanilide. The packed filters were individually dropped into a CHN elemental analyzer and measured for the percentages of carbon and nitrogen gas emitted from igniting each sample.

Table 3.4 The organic measurements in this study varied by size, characteristics, and methodologies.

Type	Abbreviation	Size fraction	Characteristics	Method
Extracellular polymeric substances	EPS	3 kDa - 0.45 µm	Colloidal fraction of proteins and polysaccharides	Bicinchoninic acid method (proteins), anthrone method (polysaccharides) (Schwehr et al., 2018)
Transparent extracellular particles	TEP	0.2 µm - 0.4 µm	Acid polysaccharides	Alcian blue staining (Passow and Alldredge, 1995)
Particulate organic carbon	POC	> 0.6 µm	% weight Carbon	CHN elemental analyzer
Chlorophyll *a*	chl *a*	> 0.6 µm	Chlorophyll *a* content within cells caught on filter	DMSO/Acetone extraction (Arar and Collins, 1997)

3.10 Statistical analysis

The data will be presented as the triplicate mean ± standard deviation. All statistical tests were conducted using built-in RStudio (Version 0.99.903) functions with spreadsheets built in Excel 2016. Student's *t*-tests were used to compare a measurement between two treatments with 95% confidence. Two-way Analysis of Variance Model (ANOVA), which utilized the Tukey's 'Honest Significant Difference' method, compared a measurement between all treatments. *P*-values <0.05 were considered significant for both tests. Due to the small sample size of three replicates, sometimes *p*-value < 0.1 is mentioned within the text.

RESULTS

4.1 Stationary growth phase experiment

Representative photographs of the four treatments used in the stationary growth phase experiment show that marine snow formed in all treatments, but to varying sizes, shapes, and counts (Figure 4.1). All four of the treatments formed visible aggregates within 24 hours (data not shown). The Control aggregates were small, spherical, and dense with smooth edges that held together during extraction. The aggregates formed in OA had fluffier edges and broke apart more easily during tank disassembly than the Controls. The WAF treatment produced irregular and elongated aggregates, with a range of sizes. The OAWAF aggregates accumulated into one to three giant masses by the end of the experiment, and the rest consisted of very small flakes. WAF and OAWAF treatments produced the largest formations over the duration of the study.

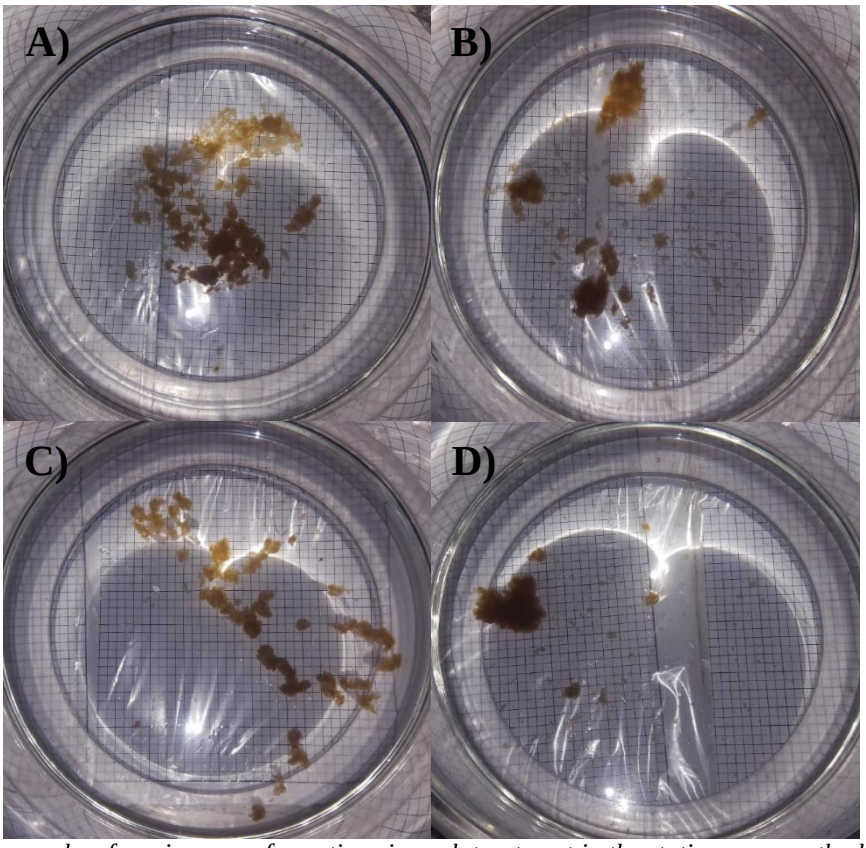

Figure 4.1 Photographs of marine snow formations in each treatment in the stationary growth phase experiment (grid squares 0.5 cm x 0.5 cm). Representative tanks: (A) Control, (B) WAF, (C) OA, and (D) OAWAF.

4.1.1 Phytoplankton biomass

Dry weight (g) was measured as total suspended solid; this was used to show the total weight present in either the SSW or AGG fractions based on the total tank volume (5.7 L) or the total volume of aggregate slurry (12 to 32 mL) pulled from the tank (Figure 4.2A). The initial OAWAF dry weights were significantly different from Control, OA and WAF ($p<0.05$). There were no significant differences between treatments within either water fraction at the ending time point (Two-way ANOVA). Combining the total dry weights from the two ending water fractions, SSW and AGG, and comparing to the total initial amount showed an overall increase in dry weight in all treatments over the duration of the experiment.

Chlorophyll *a* concentrations were expressed in total µg, similar to dry weight, to quantify *T. pseudonana* biomass accumulation from SSW to AGG (Figure 4.2B). The initial SSW chlorophyll biomass measurements showed no significant differences across treatments. The final SSW results were opposite to the initial, in that the SSW chlorophyll biomass was significantly higher in the presence of WAF ($p=0.01644$), and not the two pCO_2 levels (Two-way ANOVA, $p=0.49014$). Although the chlorophyll was not sampled from the AGG, the SSW results indicated that the majority of *T. pseudonana* cells moved from the SSW into AGG by the end of the experiment in all treatments (Figure 4.2B). WAF limited the movement of cells from SSW into AGG more than the pCO_2 level, with an average remaining SSW chlorophyll *a* of 6.06% in Control, 7.63% in OA, 13.17% in WAF, and 13.08% in OAWAF, showing that the presence of oil compounds inhibited cell aggregation.

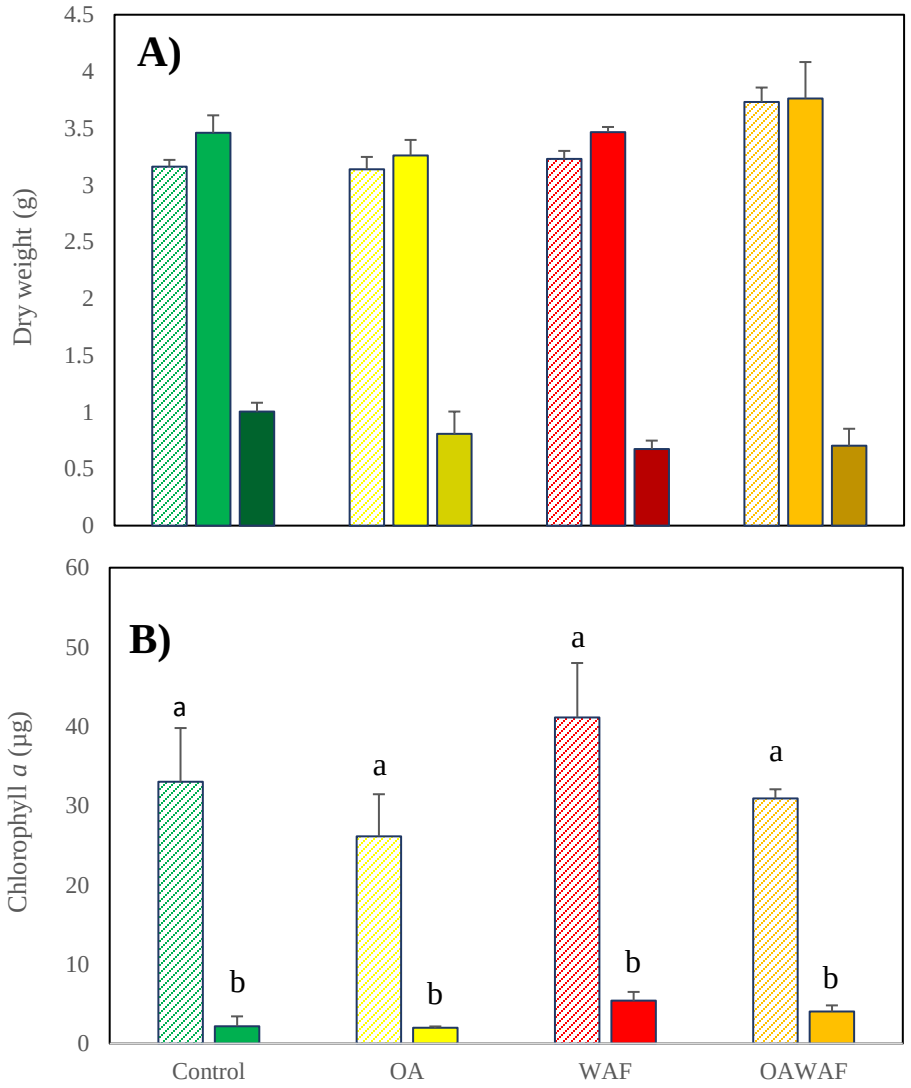

Figure 4.2 The average (A) total dry weight (g) and (B) chlorophyll a (µg) content were calculated to show changes from the beginning SSW (diagonal pattern) to the ending SSW (light solid) and AGG (dark solid) time points. Error bars show standard deviation.

4.1.2 Photophysiological response

The photophysiological response of *T. pseudonana* was determined at the beginning and end of the experiment in the SSW. Typically, F_v/F_m is used as a proxy for photosystem efficiency, but the results for all end time point replicates were below detection limits. Instead, F_vD/F_mD measurements were used (Figure 4.3A). There was no significant difference between Control and

WAF treatments (p=0.9964) due to high variability between measurements. The pCO_2-enhanced treatments (OA and OAWAF) shifted towards decreased photo-efficiency at the end of the experiment, but the variability between replicates was too high to be statistically significant (Figure 4.3A). The ending Control and WAF measurements had the highest average F_vD/F_mD and the least standard deviation (0.358 ± 0.06; 0.358 ± 0.08), indicating that the cells remaining in SSW were not as affected as those in pCO_2 enhanced treatments. The final OA and OAWAF tanks had lower average F_vD/F_mD (0.265 ± 0.14; 0.138 ± 0.14), showing a varied response potentially due to the enhanced pCO_2.

There were no significant differences between initial or final measurements in the effective PSII cross-section (σPSII) (Figure 4.3B). The final σPSII of all the treatments combined (529 ± 362 $Å^2$ $quanta^{-1}$) was larger than the initial (205 ± 16 $Å^2$ $quanta^{-1}$), consistent with *T. pseudonana*'s light harvesting capability showing stress from being in dark for 3 days (Figure 4.3B). *T. pseudonana* in OAWAF had the largest σPSII and most variability (684 ± 470 $Å^2$ $quanta^{-1}$), followed by those in OA (638 ± 280 $Å^2$ $quanta^{-1}$). The σPSII in Control and WAF treatments were smaller (376 ± 272 $Å^2$ $quanta^{-1}$; 341 ± 32 $Å^2$ $quanta^{-1}$). While not significant, there was a trend of larger antenna in OA and OAWAF than those in non-acidified conditions, Control and WAF, at the end of the experiment.

The connectivity of the photosystem (ρ) was variable across all measurements (Figure 4.3C). The cells present within oil treated tanks showed a significant difference from non-oil tanks in their ρ at the beginning time point, and by the end, trended to have less connectivity when compared to their non-oil counterpart (Two-way ANOVA, p=0.099). There were no significant differences at the final time point. WAF was lower than control but the OAWAF did not look much lower than the corresponding OA treatments.

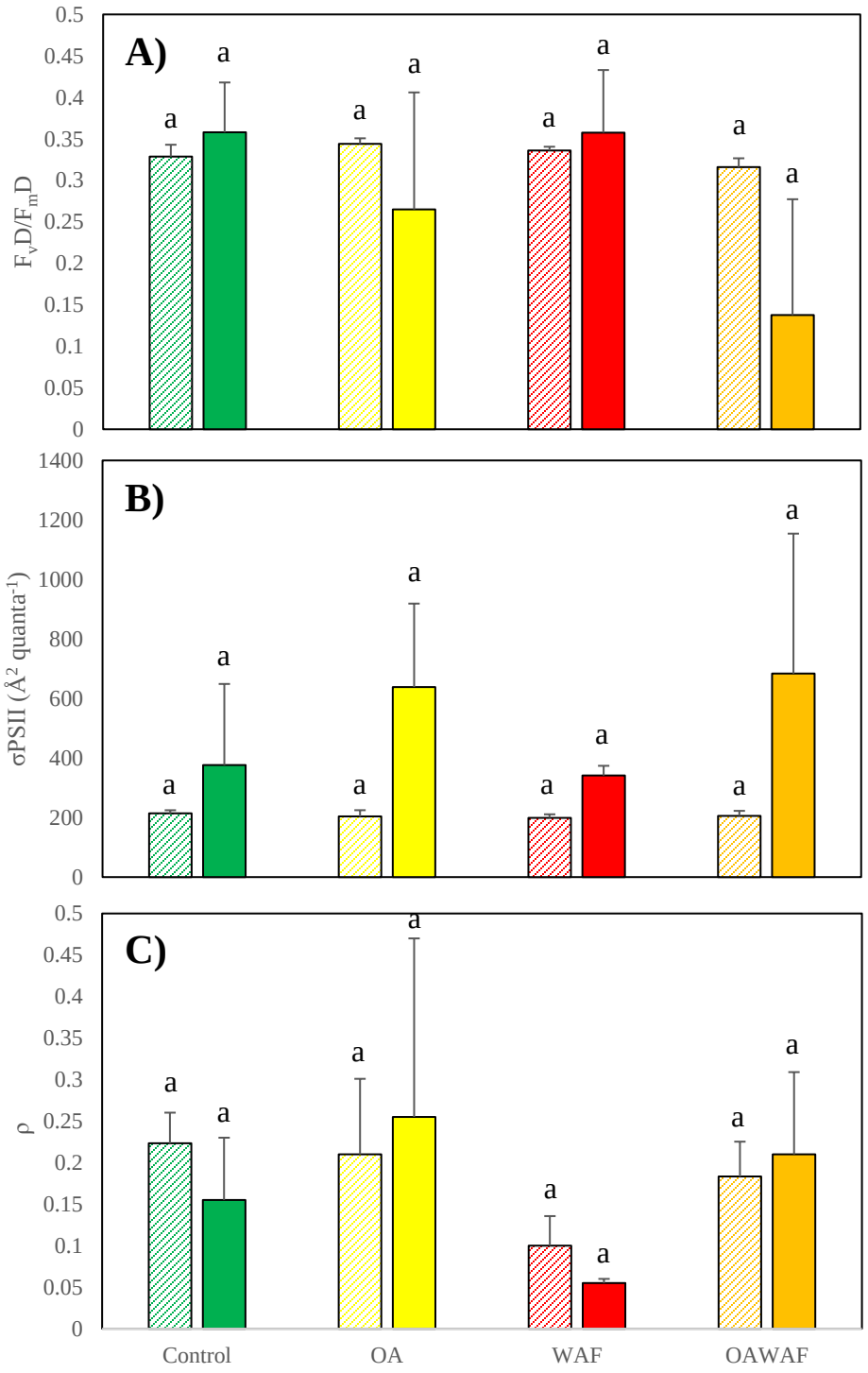

Figure 4.3 (A) PSII quantum yield (F_vD/F_mD), (B) PSII antenna size (σPSII), and (C) PSII connectivity factor (ρ) measurements were taken from the SSW in both beginning (diagonal pattern) and end (solid) time points. Standard deviation shown with error bars.

4.1.3 Aggregate formation

Image analysis of the aggregates found that there was variation in counts and sizes with treatment (Table 4.1), with WAF tanks having the most aggregates per replicate (219 ± 24 aggregates), and OA the least (78 ± 14 aggregates). Each treatment was dominated by a different size class: Control by Medium (47%), OA by Small (42%), WAF by XS (32%) and OAWAF by Large (49%) (Table 4.1). There were no Large aggregates in either Control or OA treatments (Table 4.1). OA (33.3 ± 3.4 cm^2) and OAWAF (20.1 ± 1.9 cm^2) aggregates had a lower total area of aggregate coverage than their current day counterparts did (Figure 4.4). The presence of oil shifted the aggregates towards either end of the spectrum, either XS or Large, and the enhanced pCO_2 in OAWAF showed a compound effect (Figure 4.4).

Table 4.1 The average aggregate counts and the average area of an individual aggregate separated by size class in the stationary growth phase experiment.

	Counts				Area (cm^2)			
Size	Control	OA	WAF	OAWAF	Control	OA	WAF	OAWAF
Large	0 (± 0)	0 (± 0)	2 (± 0)	1.33 (± 0.47)	0 (± 0)	0 (± 0)	6.27 (± 0.27)	8.04 (± 1.63)
Medium	9.5 (± 0.5)	5.5 (± 0.5)	4 (± 1)	0.67 (± 0.47)	2.11 (± 0.08)	2.32 (± 0.09)	2.75 (± 0)	1.39 (± 1.04)
Small	16 (± 1)	14 (± 3)	5.5 (± 0.5)	1.33 (± 0.47)	0.93 (± 0.02)	0.98 (± 0.02)	1.14 (± 0.11)	0.97 (± 0.17)
XS	56 (± 42)	58.5 (± 17.5)	208 (± 26)	135 (± 17.46)	0.15 (± 0.15)	0.12 (± 0.01)	0.07 (± 0.03)	0.06 (± 0.01)

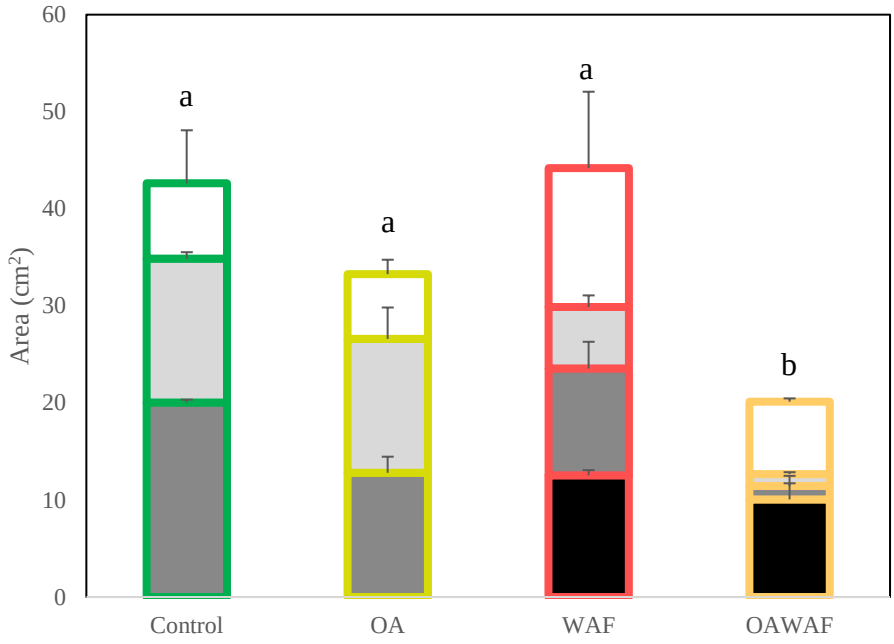

Figure 4.4 The total aggregate area sum separated by Large (black), Medium (dark grey), Small (light gray), and XS (white) average aggregate area per treatment in the stationary growth phase experiment. Standard deviation shown with error bars.

As seen in Figure 4.1, the WAF and OAWAF produced dense, opaque aggregates compared to the Control and OA treatments. This qualitative description was summarized by determining the average of each aggregates' mean gray value (Figure 4.5A). Medium aggregates were the least densely pigmented in the Control (83 ± 4.6 cm^2) treatment (Figure 4.5A). The aggregates in OAWAF were the most densely pigmented in Large (48.05 ± 10.76 optical density units), Medium (58.76 ± 2.71), and Small (71.69 ± 7.84) size classes. The aspect ratio can be used as a measure for elongation: the closer the ratio is to 1.0, the more circular the aggregate is in shape. The Large (1.35 ± 0.09), Medium (1.08 ± 0.81), and Small (1.36 ± 0.03) size classes were on average the least elongated in OAWAF (Figure 4.5B).

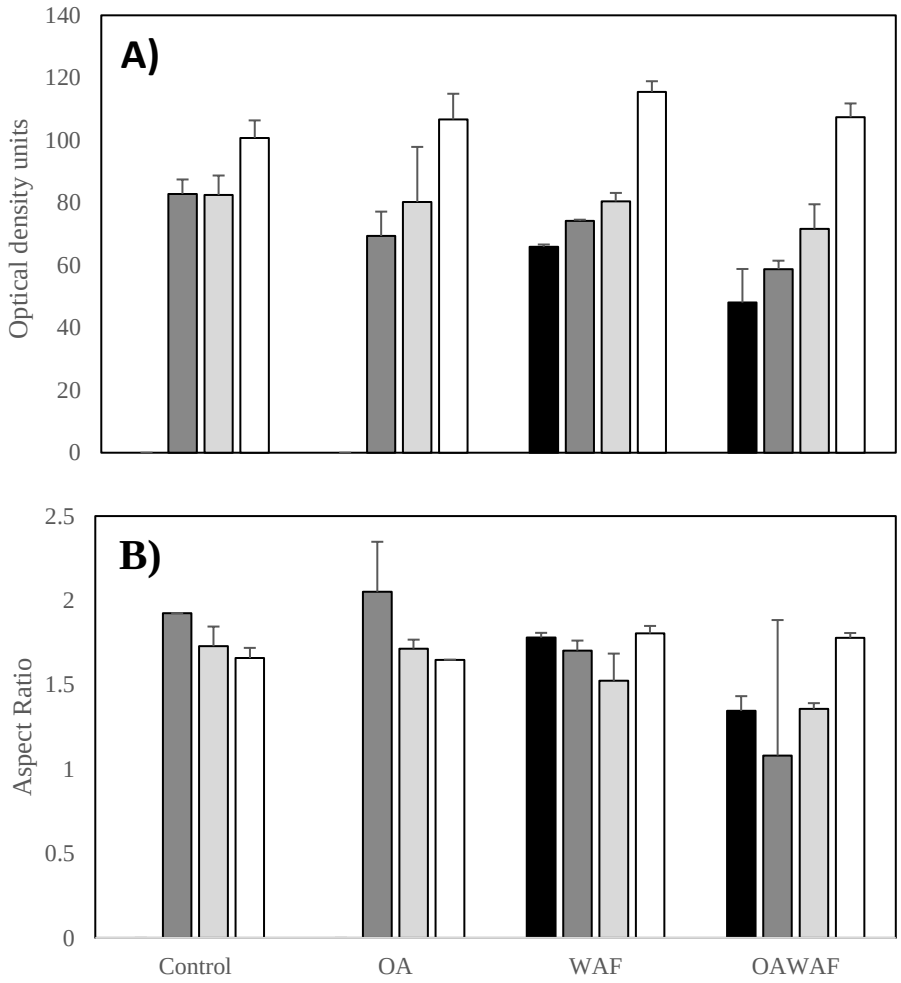

Figure 4.5 (A) The average mean gray value of all aggregates in Large (black), Medium (dark gray), Small (light gray), and XS (white) size classes in the stationary growth phase experiment. (B) The average aspect ratio of all aggregates within a size class. Standard deviation shown with error bars.

4.1.4 Exudates

Exudate were not analyzed for this portion of the study.

4.1.5 Oil analysis

The concentration of oil compounds in this experiment was measured using the EOE method only for this portion of the study. The values at the beginning of the experiment showed heterogeneity between WAF (0.74 ± 0.02 mg L^{-1}) and OAWAF (0.49 ± 0.05 mg L^{-1}) even though the treatment came from the same batch of WAF (Table 3.1). The final (at the end of three days) concentration between the two treatments was the same, and showed that the percentage lost or removed from the SSW over the duration of the experiment was higher in WAF (84%) than in OAWAF (75%).

4.2 Exponential growth phase experiment

Photographs of the six treatments used in the exponential growth phase experiment during tank disassembly showed that they produced varied aggregate sizes, shapes, and counts after 72 h (Figure 4.6). Both Control and OA treatments formed visible aggregates within 3 h, the DCEWAF and OADCEWAF treatments began producing aggregates after 24 h, and the aggregates formed the slowest in the WAF and OAWAF tanks because they only began to form after 60 h (data not shown). Therefore, the Control and OA aggregates accumulated organic material the fastest and were present for the longest amount of time in the tanks, and the WAF and OAWAF tanks the least.

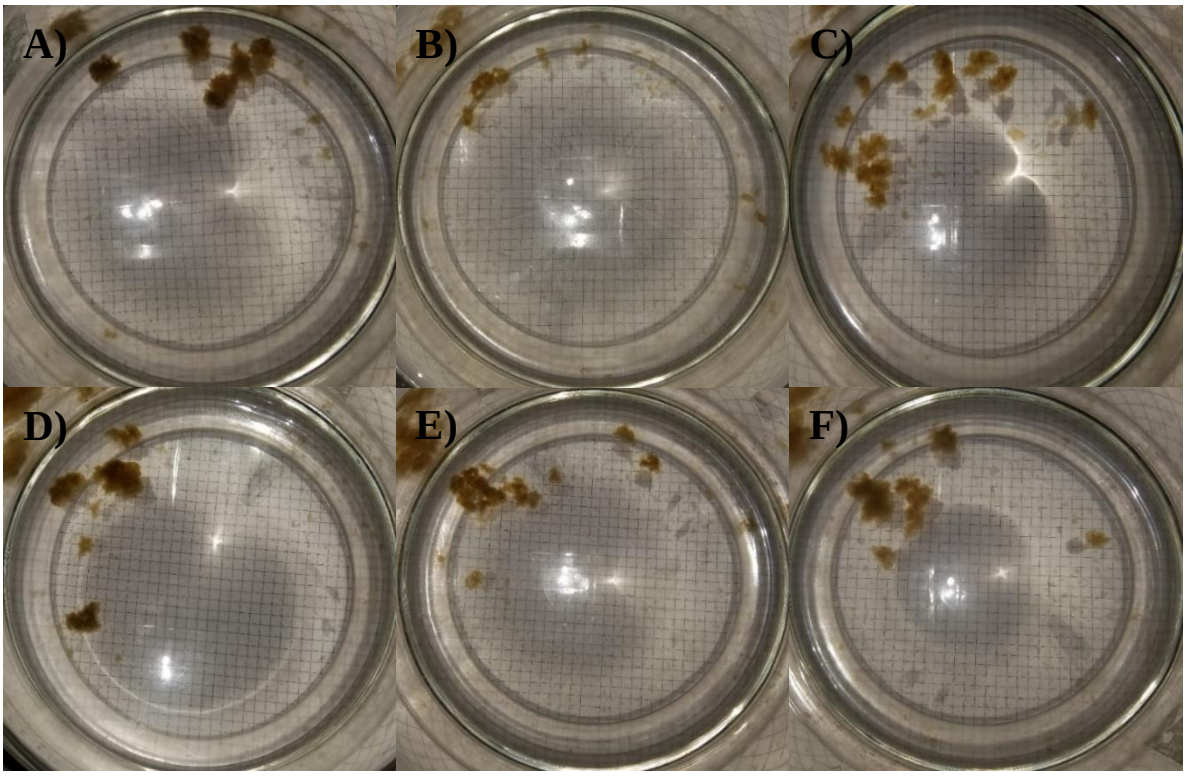

Figure 4.6 Photographs of marine snow formations in each treatment following the exponential growth phase experiment (grid squares 0.6 cm x 0.6 cm). Representative tanks: (A) Control, (B) WAF, (C) DCEWAF, (D) OA, (E) OAWAF, and (F) OADCEWAF.

4.2.1 Phytoplankton biomass

Chlorophyll *a* measurements for the exponential growth phase experiment (Figure 4.7) had similar results to the stationary growth phase experiment (Figure 4.2B). The chlorophyll was calculated to the total amount in either SSW or AGG water fractions to show cell movement into aggregate (Figure 4.7). By comparing the final time point SSW and AGG total amounts, the majority of *T. pseudonana* cells moved into aggregates in the Control (91%) and OA (93%) treatments. WAF and OAWAF treatments also showed a similar effect to the stationary growth phase experiment in that less cells accumulated within aggregates in the presence of oil compounds, 40% and 78% respectively. The DCEWAF and OADCEWAF chlorophyll *a* also

showed a decrease of cell movement to aggregate (90% and 85%), and were significantly different to their Control or OA counterpart (p=0.0233; p=0.06448). Overall, the strongest effect on chlorophyll *a* accumulation into aggregates was seen in WAF treatments, which were decreased significantly compared to the Control treatment (p=0.000819). The effect of enhanced pCO_2 on aggregate chlorophyll *a* content was negligible between Control and OA (p=0.4454) and DCEWAF and OADCEWAF (p=0.5922), but there was a significant difference between WAF and OAWAF treatments (p=0.02487). Dry weights were not measured in this experiment.

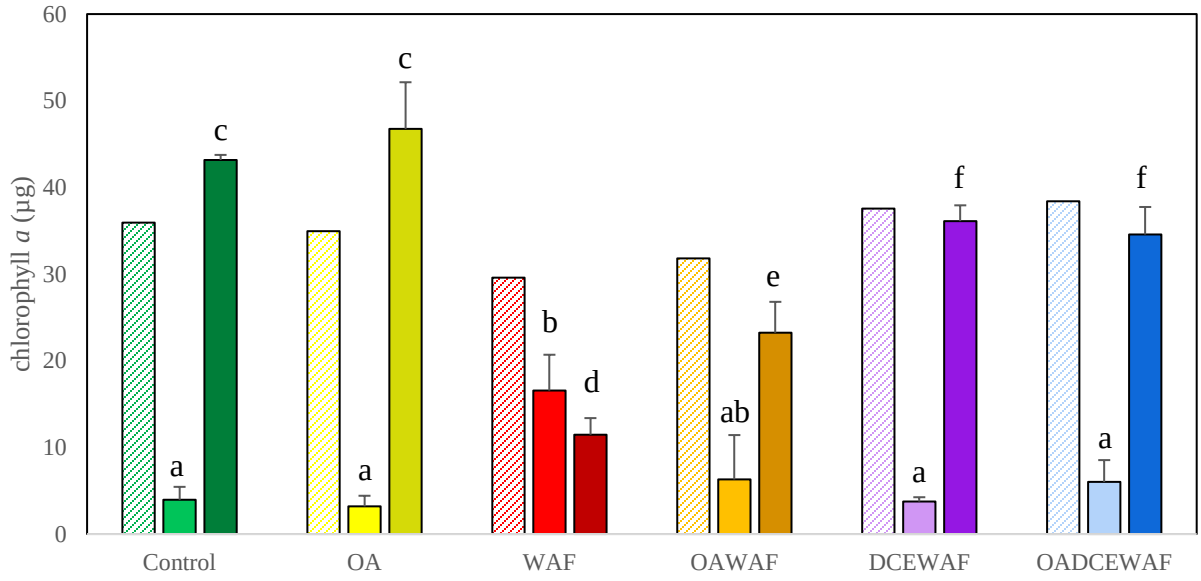

Figure 4.7 The average total chlorophyll a (µg) content was calculated for both SSW and AGG to show changes from the beginning (diagonal pattern) to the end SSW (light solid) and AGG (dark solid) time points into aggregates. Error bars show standard deviation.

4.2.2 Photophysiological response

Photophysiological measurements were taken from initial and final SSW in order to examine the stress on *T. pseudonana* over the duration of the experiment (Figure 4.8). To match the stationary phase experiment, maximum PSII quantum yield was expressed as F_vD/F_mD. There were no significant differences in photo-efficiency in any treatments at either time point (Figure 4.8A).

There was no significant difference in σPSII at the final time point between any of the treatments except in the OADCEWAF treated cells (Figure 4.8B) which had the largest and most variable σPSII between replicates (911 ± 583 $Å^2$ $quanta^{-1}$). There was trend of pCO_2 treated tanks having a larger σPSII than their associated non-acidified counterparts at the end of the period in the dark, but these were not significant (Two-way ANOVA, p=0.2647).

Final WAF (0.26 ± 0.22) and DCEWAF (0.22 ± 0.07) treatments had increased PSII connectivity factor (ρ) on average compared to the Controls (0.09 ± 0.04), with DCEWAF significantly higher (p=0.09) (Figure 4.8C). The ρ was also higher in the OAWAF (0.1 ± 0.01) and OADCEWAF (0.29 ± 0.17) treatments compared to OA (0.08 ± 0.04), but this trend was not significant (Figure 4.8C).

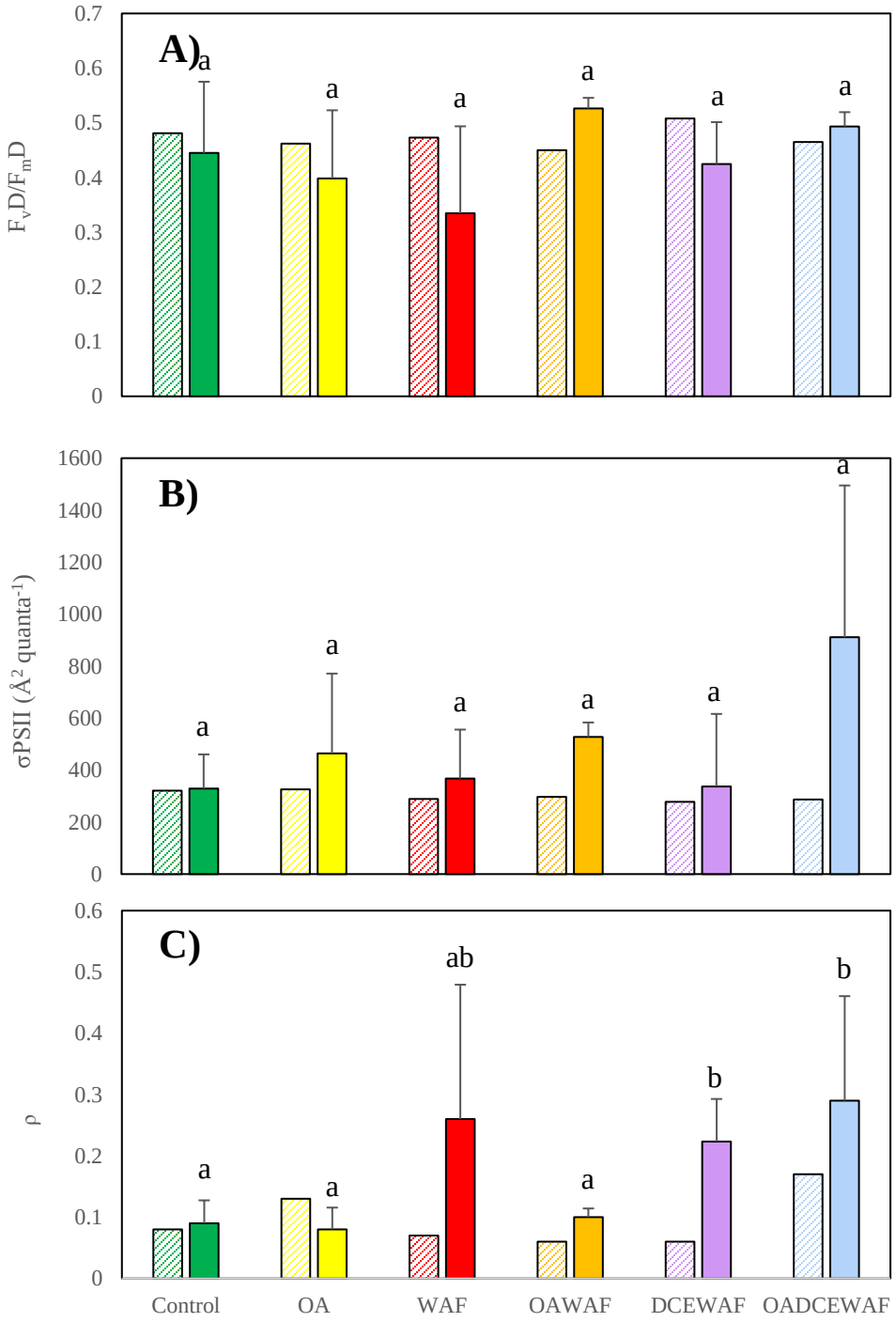

Figure 4.8 (A) PSII quantum yield (F_vD/F_mD), (B) PSII antenna size (σPSII), and (C) PSII connectivity factor (ρ) measurements were taken from the SSW in both beginning (diagonal pattern) and end (solid) time points in the exponential growth phase experiment. Standard deviation shown with error bars.

4.2.3 Aggregate formation

Individual aggregate sinking velocities were not measured. Instead, settling times for entire tanks were measured (Figure 4.9). Control aggregates settled the fastest (31 ± 6 seconds), followed by OA (53 ± 19 seconds). This trend followed through the treatments, with the OA counterpart taking a longer amount of time to settle than the current day treatments, although not significant ($p>0.05$). DCEWAF (66 ± 11 seconds) and OADCEWAF (76 ± 15 seconds) both took significantly longer to settle than Control ($p<0.04$), but not OA. WAF and OAWAF took the longest to settle, both with remaining suspended aggregates still present after 2 minutes.

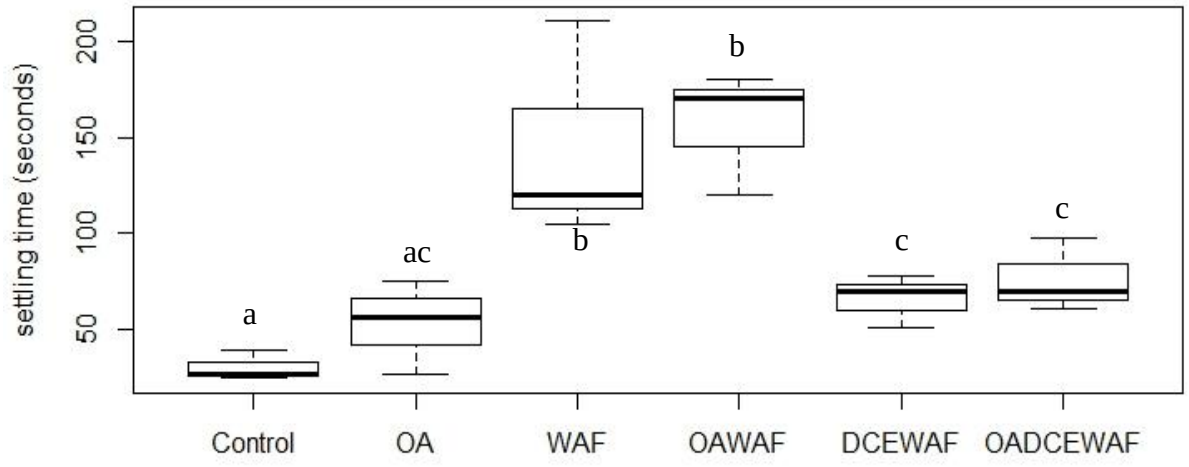

Figure 4.9 Each treatment's settling time for all aggregates during the exponential growth phase experiment was measured in seconds.

Image analysis of the aggregates found that there was also variation in counts and sizes with treatment in *T. pseudonana* kept in the exponential growth phase (Table 4.2). According to the ImageJ analysis, OADCEWAF tanks had the most aggregates per replicate (100 ± 60 aggregates), and Control the least (54 ± 9 aggregates). There were no Large aggregates in WAF

tanks, but one formed in OAWAF (Table 4.2). The Large aggregates on average covered the most tank area in DCEWAF (7.64 ± 2.73 cm^2), and the least in OAWAF (4.68 ± 0 cm^2) (Table 4.2).

Table 4.2 The average aggregate counts and the average area of an individual aggregate separated by size class in the exponential growth phase experiment.

	Counts						Area (cm^2)					
Size	Control	OA	WAF	OAWAF	DCEWAF	OADCEWAF	Control	OA	WAF	OAWAF	DCEWAF	OADCEWAF
Large	0.33 (± 0.47)	1 (± 0)	0 (± 0)	0.33 (± 0.47)	0.67 (± 0.47)	1.67 (± 0.47)	5.37 (± 0)	6.84 (± 2.20)	0 (± 0)	4.68 (± 0)	7.64 (± 2.73)	6.49 (± 1.37)
Medium	4 (± 1.41)	3 (± 1.63)	1 (± 0)	1.67 (± 0.47)	4.33 (± 1.70)	2 (± 0.82)	2.62 (± 0.03)	2.32 (± 0.39)	2.50 (± 0.70)	2.04 (± 0.30)	2.70 (± 0.12)	2.60 (± 0.74)
Small	4.33 (± 3.30)	3.33 (± 2.62)	6 (± 2.16)	6.67 (± 3.68)	4.67 (± 1.70)	3 (± 2.16)	1.02 (± 0.01)	0.82 (± 0.11)	0.84 (± 0.10)	0.85 (± 0.07)	1.06 (± 0.11)	1.04 (± 0.21)
XS	45 (± 4.08)	52.67 (± 8.06)	68.67 (± 13.3)	58.67 (± 9.81)	48.67 (± 4.11)	94 (± 56.7)	0.09 (± 0.01)	0.07 (± 0.01)	0.12 (± 0.01)	0.12 (± 0.02)	0.10 (± 0.01)	0.13 (± 0.02)

Using the ImageJ analysis, total aggregate area did not significantly change due to OA, but rather due to the absence or presence of oil compounds (Figure 4.10). The total aggregate area was highest in the DCEWAF and OADCEWAF treatments (26.39 ± 0.67 cm^2; 29.37 ± 4.10 cm^2), which correlated with the most aggregates found in the Large size class (Figure 4.10). The least total area was in the WAF and OAWAF treatments (15.52 ± 3.95 cm^2; 17.86 ± 1.26 cm^2), where the aggregates skewed towards smaller size classes than the other treatments (Figure 4.10). The

presence of WAF and DCEWAF produced significantly more XS aggregates than the non-oiled tanks, with the most amount in OADCEWAF (11.54 ± 5.41 cm^2). The Control and OA treatments had the least amount of XS area (4.03 ± 0.43 cm^2; 3.58 ± 0.29 cm^2). OA enhanced the accumulation of organic material into Large across all treatments when compared to their control counterparts (Figure 4.10). In current day conditions, the Medium size class had a greater sum of aggregate area (10.54 ± 3.80 cm^2).

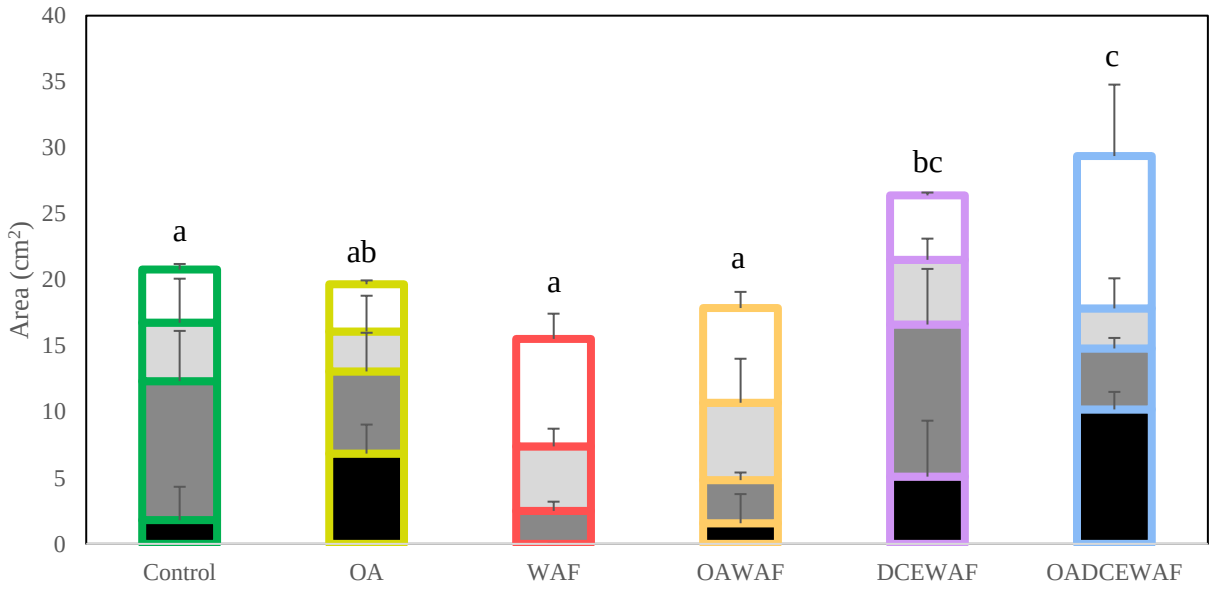

Figure 4.10 The total aggregate area sum separated by Large (black), Medium (dark grey), Small (light gray), and XS (white) average aggregate area per treatment. Standard deviation shown with error bars.

Control and OA aggregates visually appear denser and more tightly packed based on their darker pigmentation (Figure 4.6). To quantify that, the mean grey value (calibrated units of optical density) of each aggregate was used to compare aggregate densities across size classes and

treatments (Figure 4.11 A). OA Large (47.97 ± 7.49) and Control Medium (55.35 ± 7.50) and Small (69.93 ± 3.96) aggregates were the densest among all treatments. XS aggregates were similar across all treatments, but the least dense and most variable within Control tanks. The OADCEWAF treatment on average produced the highest total Large aggregate area (Figure 4.10), but they were the least dense among the treatments (Figure 4.11A). The Medium aggregates were less dense in oil treated tanks, but not different between OA levels.

According to the aspect ratio of the aggregates, the medium size class was the most elongated overall in WAF and OAWAF (Figure 4.11B). Control and OA were the least elongated as their aspect ratio was closer to 1.0 than the other treatments (Figure 4.11B). The OA Large (1.41 ± 0.04) size class was more circular, or closer to 1.0, than the Controls (1.75 ± 0), but there was also only a single Large aggregate between the Control triplicates. The presence of oil compounds produced more variability between size classes. OADCEWAF had the least circular Large aggregates (1.92 ± 0.46). WAF (1.96 ± 0.34) and OAWAF (2.12 ± 0.38) both had elongated Medium sized aggregates (Figure 4.11B). Small aggregates were elongated in the presence of oil. There was no discernable trend to the shape of the flakey XS size class, which may simply be due to the nature of their size (Figure 4.11B).

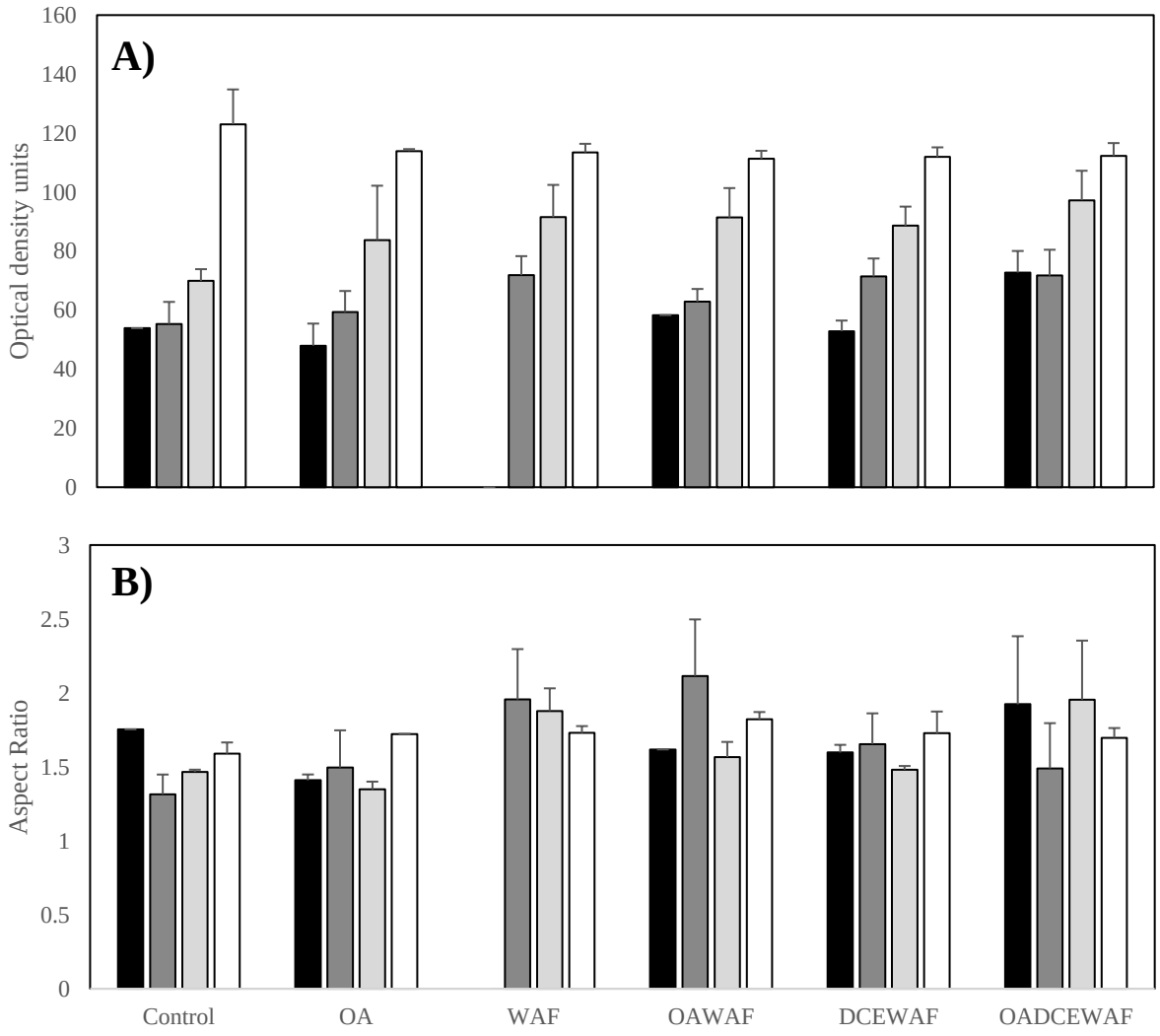

Figure 4.11 (A) The average mean gray value of all aggregates in Large (black), Medium (dark gray), Small (light gray), and XS (white) size classes for the exponential growth phase experiment. (B) The average aspect ratio of all aggregates within a size class. Standard deviation shown with error bars.

4.2.4 Exudates

Colloidal EPS was measured as the sum of proteins, neutral sugars, and uronic acids from SSW (between < 0.7 µm and > 3 kDa), and particulate EPS was measured using unfiltered AGG (Figure 4.12). The colloidal EPS was heavily dominated by proteins in all treatments compared to total carbohydrates (total carbohydrates = neutral sugars + uronic acids), and the ratio did not vary

significantly between treatments ($p>0.05$) (Figure 4.13). Rather, what varied between treatments was the total amount of colloidal EPS in the SSW. Control (1.17 ± 0.23 mg) and OA (1.01 ± 0.23 mg) treatments had the least amount of total colloidal EPS remaining in the SSW, whereas WAF (1.60 ± 0.34 mg), OAWAF (1.63 ± 0.09 mg), DCEWAF (1.52 ± 0.35 mg) and OADCEWAF (1.96 ± 0.32 mg) were all increased (Figure 4.12A). However, despite the differences in EPS quantity, Control was not significantly different from OA, WAF or DCEWAF, but OA was significantly different from OAWAF and OADCEWAF ($p<0.05$).

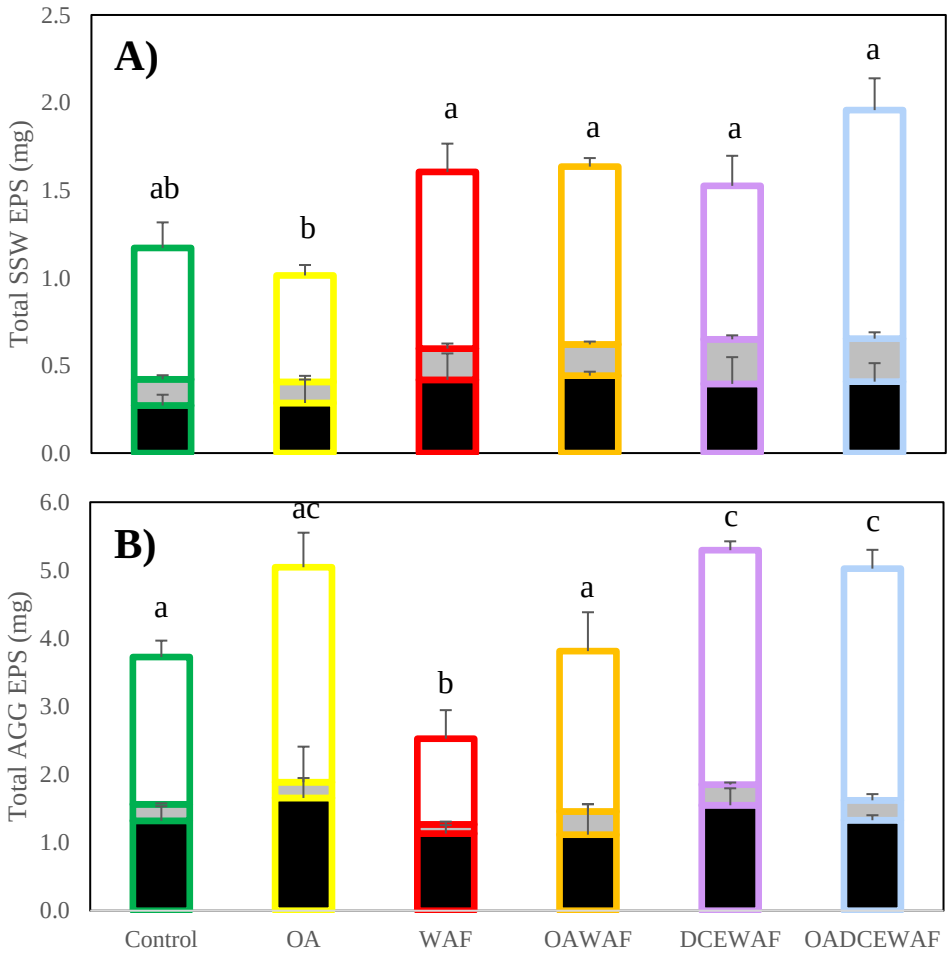

Figure 4.12 The average total (mg) neutral sugars (black), uronic acids (grey), and proteins (white) stacked to show total content of colloidal EPS in (A) SSW and particulate in (B) AGG.

The proteins, neutral sugars and uronic acids were also measured in the AGG, but because the cells were not excluded, it is referred to as the particulate EPS. This fraction, like SSW, was also dominated by proteins (Figure 4.13). The most total particulate EPS (Figure 4.12) collected in AGG was in DCEWAF (5.30 ± 0.40 mg), which was significantly different from the Control (3.73 ± 0.45 mg) treatment ($p<0.05$). The least amount of particulate EPS was in the WAF (2.53 ± 0.57 mg) treatment, which also had the lowest ratio of proteins-C to carbohydrates-C in AGG (1.18 ± 0.25).

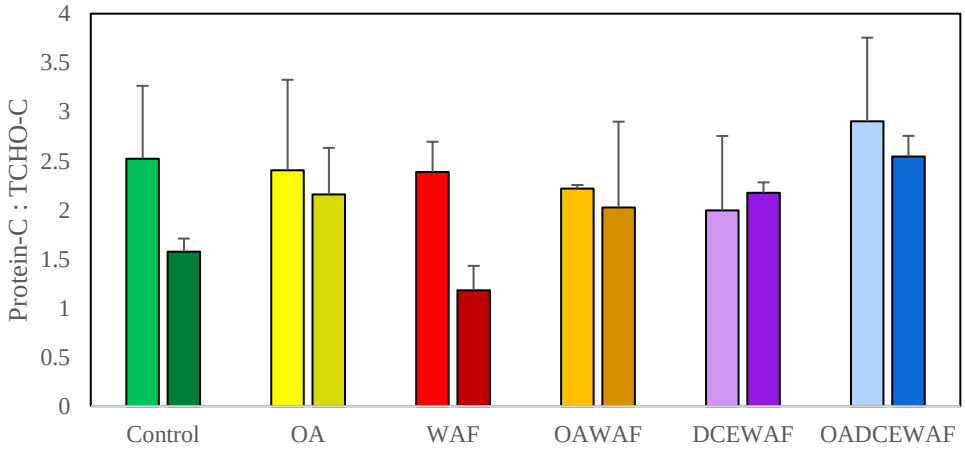

Figure 4.13 The average stickiness ratio of proteins-C to total carbohydrates-C in SSW (light) and AGG (dark) fractions. Error bars show standard deviation.

The AGG ratio of proteins-C to carbohydrates-C was significantly higher in DCEWAF (2.17 ± 0.11) and OADCEWAF (2.54 ± 0.21) than in Control (1.57 ± 0.13) ($p<0.01$), but not significant between any other treatment. OADCEWAF had the highest amount of AGG proteins-C to carbohydrates-C (2.54 ± 0.21 mg C-equivalents L^{-1}) (Figure 4.13). There was a trend of higher

proteins-C to carbohydrates-C in OA, OAWAF and OADCEWAF compared to their current day counterpart, but this was not significant.

Total SSW TEP was higher in WAF (3.86 ± 0.35 mg Gxan) and OAWAF (3.90 ± 0.47 mg Gxan) treatments than in Control (1.36 ± 0.08 mg Gxan) or OA (1.20 ± 0.15 mg Gxan). TEP was not measured in the AGG fraction, or in the SSW of DCEWAF or OADCEWAF. TEP was significantly affected by the presence of oil ($p<0.01$), but not between the two pCO_2 conditions (Figure 4.14).

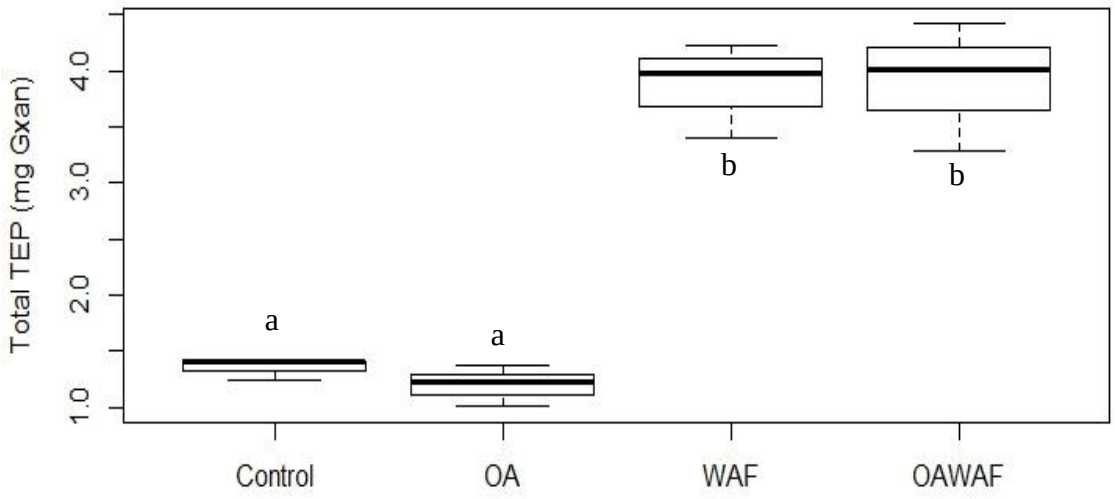

Figure 4.14 The total TEP was determined in the SSW for Control, OA, WAF, and OAWAF. DCEWAF and OADCEWAF were excluded from this measurement.

4.2.5 Oil analysis

The EOE at the beginning of the exponential growth phase experiment was similar between WAF and DCEWAF, which indicated that the dilution was successful (Table 3.1). The final (at the end of three days) EOE concentration indicated that the most removed or lost from the SSW was in OADCEWAF (72%), and the least in DCEWAF (8.4%).

Due to the innate heterogeneity of EOE measurements, PAH extractions were used for a thorough analysis of how these toxic compounds partitioned between the SSW and AGG. Initial PAH concentrations were significantly higher in both WAF (61.27 mg L^{-1}) and OAWAF (60.29 mg L^{-1}) than in DCEWAF (2.75 mg L^{-1}) and OADCEWAF (2.56 mg L^{-1}) ($p<0.01$), demonstrating that WAF treatments exposed *T. pseudonana* cells to more of the toxic oil compounds than DCEWAF treatments (Figure 4.15). WAF (1.50 ± 0.83 mg L^{-1}) and OAWAF (2.39 ± 0.25 mg L^{-1}) incorporated more PAHs into AGG than DCEWAF (1.38 ± 0.08 mg L^{-1}) or OADCEWAF (1.19 ± 0.14 mg L^{-1}) (Figure 4.15). There were no significant differences caused by pCO_2 levels ($p>0.05$).

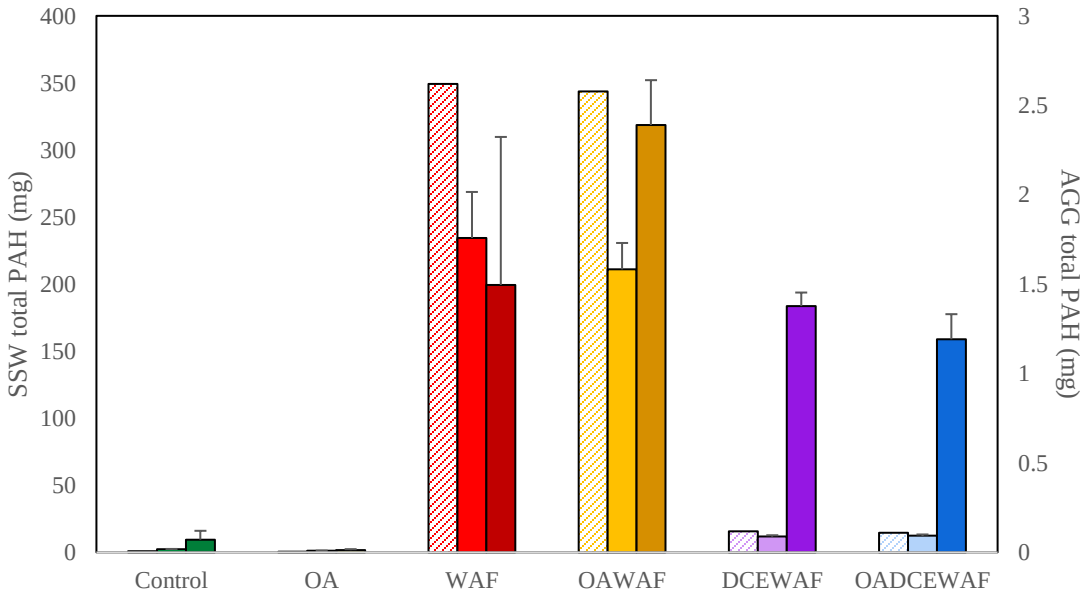

Figure 4.15 The total PAH (mg) was measured in the beginning SSW (diagonal pattern), end SSW (light solid) and AGG (dark solid). Standard deviation shown with error bars. The SSW and AGG (mg) measurements are on different scales.

Even though the starting PAH concentration was lower in DCEWAF and OADCEWAF treatments than in WAF, and more PAHs overall moved into AGG in WAF and OAWAF treatments, a significantly higher percentage moved from SSW into AGG (8.78% and 8.16%), than in WAF (0.43%) or OAWAF (0.70%) ($p<0.05$) (Figure 4.16). Based on final time point measurements, WAF and OAWAF tanks both experienced a significant loss over the duration of the experiment, 32.5% and 37.9% respectively, by degradation or sticking to the glass walls of the tanks (Figure 4.16). The loss cannot be associated with photo-degradation because the experiment was conducted in total darkness. DCEWAF and OADCEWAF also lost PAH concentrations of 15.7% and 6.6% respectively.

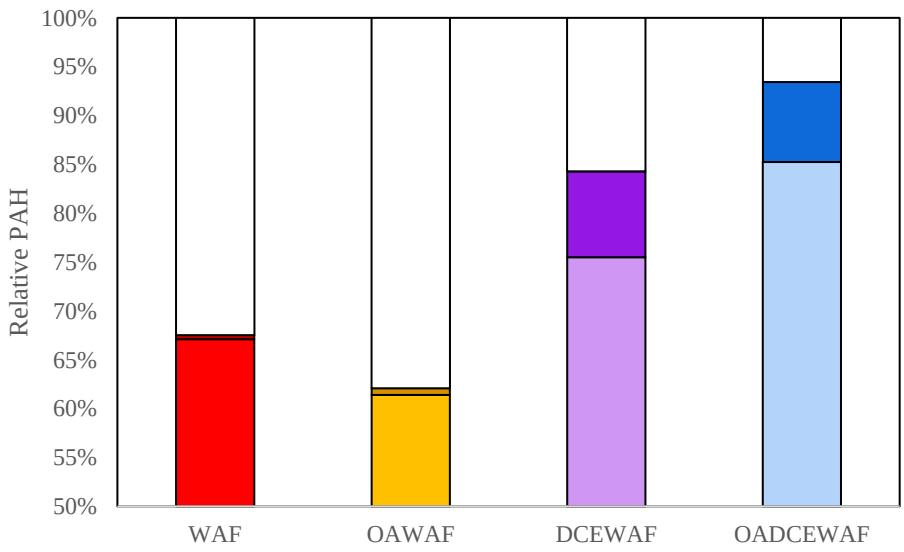

Figure 4.16 The average relative PAH percentage that was lost (white) over the duration of the experiment, incorporated into AGG (dark solid), or remained in SSW (light solid) was calculated based on the initial SSW measurements.

Based on total aggregate area measured with image analysis, a higher average amount of PAHs were incorporated per cm^2 in WAF (0.0963 mg cm^{-2}) and OAWAF (0.1338 mg cm^{-2}) treatments, meaning there was a higher concentration within them than in DCEWAF (0.0522 mg cm^{-2}) or OADCEWAF (0.0406 mg cm^{-2}) (Figure 4.17). Therefore, WAF aggregates, although less abundant and smaller, scavenged an overall greater amount of PAH compounds per aggregate area than DCEWAF aggregates (Figure 4.17). DCEWAF treatments formed larger aggregates with less mg PAH cm^{-2}, but actually removed a higher relative percentage from the SSW to aggregate (Figure 4.16).

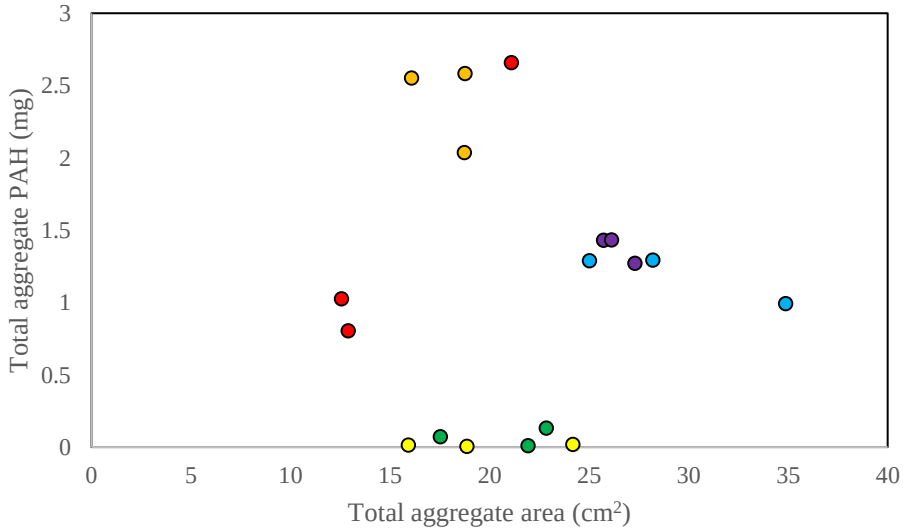

Figure 4.17 The total PAH (mg) incorporated into the total aggregate area (cm^2) for each replicate of the Control (green), OA (yellow), WAF (red), OAWAF (orange), DCEWAF (purple), and OADCEWAF (blue).

DISCUSSION

Diatoms are a diverse group of phytoplankton, each with the potential to respond uniquely to ocean acidification or oil spills. They are essential for the biological carbon pump because of their high abundance and primary productivity rates (Tre'guer et al., 1995; Mann, 1999). While previous work has shown that phytoplankton species have individual responses and overall growth rate is reduced in oil spill conditions, the relative abundance of diatoms actually increased following DwH spill (Parsons et al., 2015; Bretherton et al,. 2018). Their subsequent contribution to marine oil snow formation is thought to have influenced the fate of the oil (Yan et al., 2016; Passow et al., 2019). Future ocean conditions are likely to change as increasing anthropogenic CO_2 affects the carbonate chemistry, and may ultimately influence phytoplankton exudate production and contribution to marine snow. Many studies have shown that OA affects growth rate and photophysiology across different species and sizes of diatoms (Tortell et al., 2008; Li et al., 2012; Wu et al., 2014), alluding to an unpredictable and variable future. This study used a multifactorial laboratory experiment to examine the impact that ocean acidification may have on marine snow and marine oil snow formations.

EPS and TEP are amphiphilic macromolecules released into the environment by microbial organisms and are essential for aggregation and the biological carbon pump (Passow and Carlson, 2012). Changes in the composition and amount of exudates released by microorganisms may ultimately affect the carbon flux when considering that recent understanding of exudate stickiness revolves around the protein to carbohydrate ratio (Santschi, 2018; Schwehr et al., 2018). Riebesell et al. (2007) speculated that more TEP may be released in future ocean conditions, and could potentially result in increased aggregation. Others have found that because TEP are buoyant

particles, a higher proportion accumulated within aggregates slows their sinking rates, so increased TEP may not actually increase the carbon flux (Mari, 2008). TEP will stay suspended in surface waters unless the particles attach to heavier materials, which are denser than water, like cells or minerals (Mari et al., 2017). The stickiness of these macromolecules may be affected by changing ocean conditions (Mari, 2008), so there is the potential for compounding effects to the biological carbon pump.

This experiment measured the sum of proteins, neutral sugars and uronic acids released by *T. pseudonana* as colloidal EPS and the stainable acid polysaccharides as TEP. These results indicated that OA did not enhance *T. pseudonana*'s release of exudates into the environment. This may be due to *T. pseudonana* not being significantly affected by the increased availability of DIC, shown in this experiment and others (McCarthy et al., 2012), and because the experiment occurred in the dark where new photosynthetic products could not be generated. A 100-day study also found that *T. pseudonana* grown in 760 ppm showed no significant change in F_v/F_m or σPSII, and overall very little long-term effects (Crawfurd et al., 2011). While no significant change in F_v/F_m was observed in the present study, the increase in σPSII measured at the end of the experiment was associated with the dark incubation rather than either the OA or oil or oil plus dispersant treatments. If the intracellular processes did not change due to OA, then *T. pseudonana* may not have produced different macromolecules to exude. An examination of protein and total carbohydrate concentrations and ratios revealed that OA did not influence these parameters. A similar roller table experiment using *Thalassiosira weissflogii*, a larger diatom related to *T. pseudonana*, also found that OA did not enhance TEP production (Seebah et al., 2014). However, Thornton (2009) noted that lower pH did not affect TEP, but instead caused *Chaetoceros muelleri*

to reduce F_v/F_m and release more total carbohydrates in low molecular weights rather than exopolymers (Thornton, 2009). Hence, findings can be species specific.

The EPS and TEP results build on previous studies that the presence of oil and oil plus dispersant, in this case in the form of WAF and DCEWAF respectively, affects exudate release and aggregation. The total amount of neutral sugars, uronic acids and proteins left suspended in the SSW was higher in all treatments with oil compounds present. This matches previous experiments that have shown phytoplankton release EPS in response to stress (Quigg et al., 2016), and that *T. pseudonana* is a species particularly affected by oil (Bretherton et al., 2018). EPS are amphiphilic molecules, similar to chemical dispersants, which decrease the surface tension of water and can interact with oil (Quigg et al., 2016; Schwehr et al., 2018). These organic materials may even be more efficient than synthetic surfactants at dispersing oil by forming micelles (Schwehr et al., 2018), and have been shown to emulsify and incorporate oil (Quigg et al., 2016; Hatcher et al., 2018; Xu et al., 2018a; Passow et al., 2019). There was more TEP left in the SSW in WAF and OAWAF than in Control or OA treatments, which may have been the high amount of very small, flake aggregates that were buoyant and did not sink during tank disassembly. These micro-aggregates (possibly the same observed by Doyle et al., 2018 but further studies required) stayed suspended even after the tanks were allowed to settle out, so they were reincorporated into the SSW fractions. It is interesting that even though WAF and OAWAF produced different sized aggregates, the two treatments had similar remaining TEP in the SSW. TEP was not measured in DCEWAF or OADCEWAF (as the protocol does not work in the presence of Corexit), but the EPS measurements showed that these treatments enhanced exudate production. The petro-carbon concentration was lower in DCEWAF, but the presence of Corexit may have affected the cell walls and allowed internal material to leak (pers. observation).

The results of the aggregate image analysis suggest that OA may affect the carbon flux, and consequently the biological carbon pump. The total amount of proteins, carbohydrates, and chlorophyll *a* that accumulated in the aggregates did not vary significantly between current and future pCO_2 levels, but because larger aggregates contribute a significant amount of POC to the seafloor (Smetacek, 1985), and sink faster than diatom cells alone (Culver and Smith, 1989) or smaller aggregates (Daly et al., 2016; Passow et al., 2019), more organic matter may ultimately sink. Multifactorial designs such as this experiment are helpful for adding to the greater body of knowledge on how OA may affect the biological carbon pump, but it is difficult to compare these findings to others due to the variation in experimental designs and species studied, and conflicting conclusions. For instance, there are discrepancies from one study to another on which phytoplankton will be the dominant species in the future. Some studies suggest that the change in temperature and nutrients will lead to smaller species dominating (Bopp et al., 2005; Morán et al., 2010), while others predict that the increase of DIC may positively affect larger species (Wu et al., 2014). Even within this study, the stationary and exponential growth phases of *T. pseudonana* produced variable aggregate formations with the same treatments. The trends were similar, with OA producing larger aggregates than current pCO_2 conditions, but the details varied beyond that. These differences may be because there were more exudates present in the stationary growth phase culture when it was added to the roller tank (Thornton, 2002).

The WAF and DCEWAF treatments affected exudate production, aggregate size distribution, shapes, and sinking rates The concentrations of oil used in this study were well below the 200 mg L^{-1} limit to simulate authentic spill conditions (Bejarano et al., 2014), as has been a critique among some recent oil toxicity work (Wade et al., 2017). The DCEWAF treatments used in the exponential growth phase experiment were set to levels even more dilute than in other studies

(Passow et al., 2017; Wade et al., 2017) in an attempt to reach similar concentrations as the WAF. This dilution also benefitted the study because it has been documented that *T. pseudonana* is very sensitive to concentrated CEWAF treatments (Bretherton et al., 2018). These treatments were effective at initiating a response from the diatoms without immediately incapacitating them, but still at a high enough dose to be environmentally relevant.

WAF treatments produced varied aggregate formations between the two tested growth phases of *T. pseudonana*. A stationary culture is similar to an end stage of an algal bloom in that there is more pre-existing exuded organic material available for aggregation, making older cultures beneficial for aggregation experiments. The stationary phase experiment lost more petro-carbons from the SSW than the exponential growth phase experiment (EOE, Table 3.1). This combined with the stark differences in aggregates shows that responses can change even within the same strain of algae (Figures 4.1 and 4.6), and may ultimately affect oil accumulation and sedimentation potential. Passow et al. (2017) also noted that findings were determined by the growth phase of the algal cultures prior to starting experiments.

The PAH analysis of the exponential growth phase experiment revealed that there were differences between WAF and DCEWAF of the amount that migrated from SSW into aggregates. PAHs were of particular interest because they are known to last for years after a spill and are some of the most toxic components of crude oil to marine organisms (Meador, 2003; Abbriano et al., 2011; Sammarco et al., 2013). Hatcher et al. (2018) found that the addition of Corexit dispersant led to more oil compounds accumulating within marine oil snow. This was similar to the current study where total relative incorporation of PAHs was higher in DCEWAF than WAF. There was more aggregate area and a lower concentration of PAHs in DCEWAF than WAF, so perhaps there was lower ratio was more efficient at scavenging oil compounds. Previous marine oil snow studies

have shown that aggregates have a maximum carrying capacity for oil compounds (Passow et al., 2019), and that Corexit increases the oil accumulated in aggregate (Passow et al., 2017). The DCEWAF concentration was also lower than in other similar studies, which may explain discrepancies on the effects on aggregation and that Corexit may inhibit oil accumulation (Xu et al., 2018a).

The exponential growth phase experiment did not show that DCEWAF inhibited aggregate formations, but rather that WAF did. The aggregate chlorophyll *a* showed that even though there was more EPS production and total area in the DCEWAFs than Controls, more cells were left suspended in the SSW. This may be associated with the denser aggregates found in Controls than in DCEWAF (Figure 4.11A), which can also be seen when directly comparing total chlorophyll *a* to total aggregate area (Figure 5.1). This decreased diatom aggregation has previously been correlated with the presence of Corexit (Passow et al., 2017).

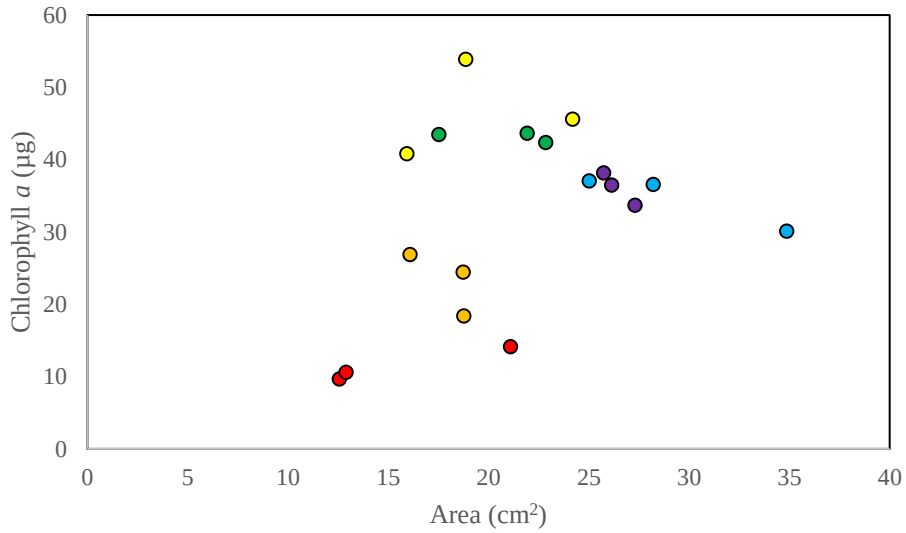

Figure 5.1 The average area (cm^2) and chlorophyll a *(µg) for the aggregates in Control (green), OA (yellow), WAF (red), OAWAF (orange), DCEWAF (purple), and OADCEWAF (blue) in the exponential growth phase experiment.*

Individual aggregate sinking velocities were not measured, but the average calculated equivalent spherical diameter (mm) and sinking velocity (m d^{-1}) from each size class in the exponential growth phase experiment showed no significant separation between treatments (Figure 5.2). However, the fastest calculated average sinking aggregates were in either DCEWAF or OADCEWAF in each size class, which did not match the timed settling rates of entire tanks (Figure 4.9) where Control and OA were the fastest. This discrepancy may be a result of the density (Figure 4.11A) of Control and OA aggregates, which were more compact with cells (Figure 5.1) that assist in ballasting marine snow (Thornton, 2002), or potentially because the DCEWAF and OADCEWAF had more XS aggregates that are buoyant and sink slowly (Table 4.2). This diverges from previous studies that suggests that oil compounds increase the density and sinking velocities of aggregates (Passow et al., 2019). It is important to note, as it may need to be incorporated into future modeling efforts that bio volume is more representative of aggregate sinking than area.

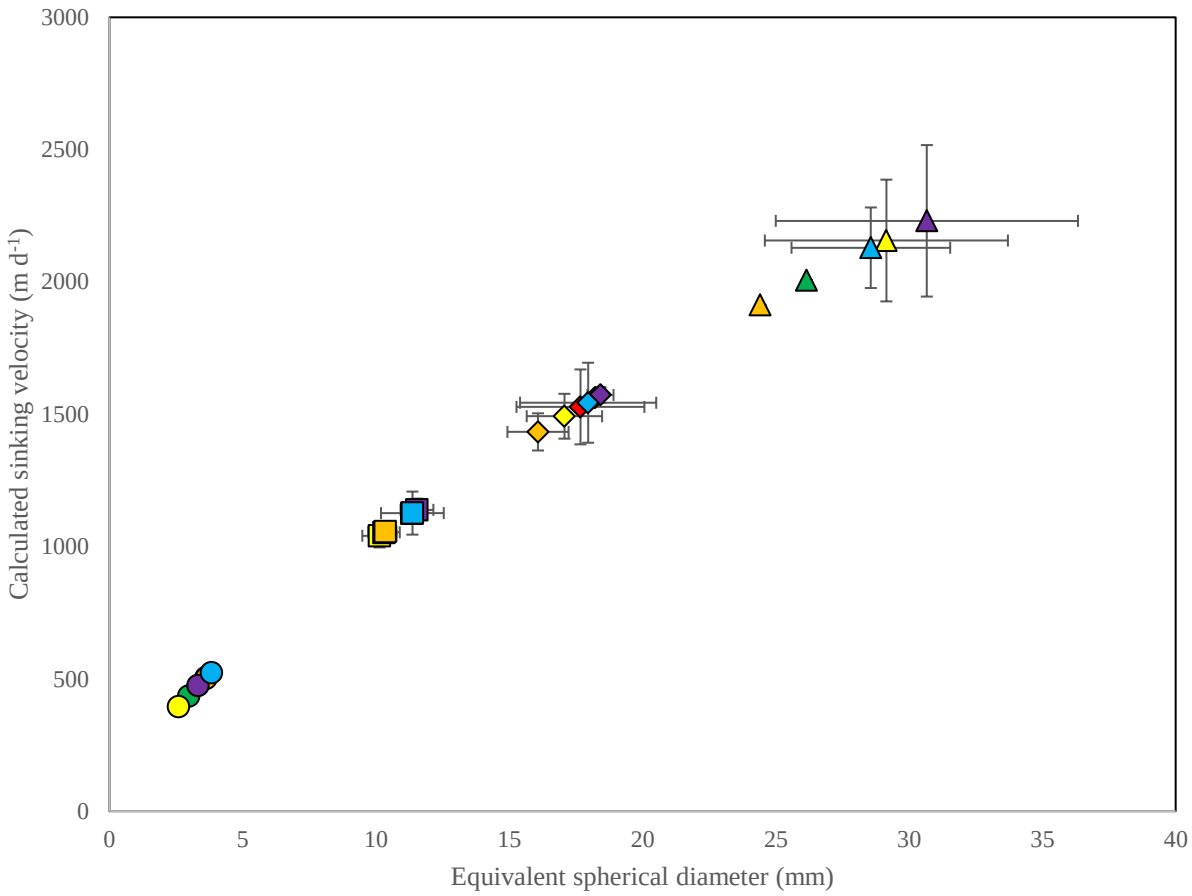

Figure 5.2 The average equivalent spherical diameter (mm) and the calculated sinking velocity (m d^{-1}) for Large (triangle), Medium (diamond), Small (square), and XS (circle) aggregates in the exponential growth phase experiment. The Control (green), OA (yellow), WAF (red), OAWAF (orange), DCEWAF (purple), and OADCEWAF (blue) are separated within size class.

During tank disassembly and aggregate extraction, the WAF and OAWAF aggregates broke apart extremely easily. This complicated removing intact formations from the tanks in a way not seen in the other treatments. Interestingly, the DCEWAF and OADCEWAF aggregates, while less dense than Control or OA, held together the best of all the treatments during aggregate removal. The divergence between the two oil treatments may be due to the EPS protein-C to carbohydrate-C ratio measured in the aggregates, where DCEWAF was higher than WAF. The

ratio of protein-C to carbohydrate-C has been determined as a proxy for stickiness and is associated with lowered surface tension (Santschi, 2018; Schwehr et al., 2018; Xu et al., 2018a; Xu et al., 2018b). This ratio for *T. pseudonana* EPS is naturally higher than other phytoplankton, and therefore is more hydrophobic in nature (Zhang et al., 2012; Chui et al., 2019). This hydrophobicity may be why the aggregates were not dispersed by the Corexit in DCEWAF, contrary to other studies (Xu et al., 2018a), and instead may enhance EPS aggregation (Chiu et al, 2019). The WAF aggregates had the lowest ratio, meaning the least sticky, and the least amount of aggregates produced in the experiment. Previously, Coomassie stained particles (CSP), or protein exudates, were not determined essential for aggregation (Cisternas-Novoa et al., 2015). Instead, the focus of published aggregation research was on TEP (Thornton, 2002; Passow and Carlson, 2012; Mari et al., 2017). These results build on the developing knowledge of the importance of proteins for marine snow formations.

Additionally to the composition of organic molecules present in the water, the pH within the system is also important to aggregation. The aggregated material in this experiment showed a trend of increased protein-C to carbohydrate-C ratio for stickiness in OA treatments, which correlated with the larger aggregates seen in these enhanced pCO_2 conditions treatments, but was not significant (Figure 4.12). The lower pH in these treatments means that hydrogen ions are present in higher concentrations than in the ambient conditions studied. These ions are important for hydrogen bonding and affect how organic molecules interact, such as the non-covalent bonds formed between proteins and polysaccharides that maintain molecular shape (Schwehr et al., 2018). The shift in pH used in this study may have contributed to the larger formations and higher accumulation of exudates within aggregates. The potential for OA to increase aggregate formation (Riebesell et al., 2007) and carbon flux (Wu et al., 2014) has also been proposed by other studies.

Effective greenhouses gas management is essential moving forward to limit the advancement of ocean acidification and the other effects of climate change. Studies like these are beneficial for understanding marine snow formation in current conditions, but can also reveal insights to the response of harmful conditions like oil spills or different carbonate conditions. It is important to note that these laboratory-controlled studies have their limitations, and extrapolating to implications can be complex. The study would have benefitted from more tank replicates, additional treatments, and a diverse range of species tested for a more comprehensive investigation. However, these experiments are difficult to repeat because they are both time and resource intensive, and the work presented here could not have been completed without collaboration. Furthermore, while the results of this study are intricate, they provide evidence that ocean acidification may impact aggregation and carbon transportation, and that the growth state and exudate presence may elicit varying responses.

CONCLUSIONS

Overall, this study adds to the current knowledge on aggregation, marine oil snow, and the impacts of ocean acidification. Based on the aggregate area and morphology, it was determined that OA affected aggregate formations, and subsequently may affect the biological carbon pump. It has been suggested that a shift towards larger phytoplankton may occur in the future due to the increased DIC diffusing into cells and decreasing carbon limitation (Wu et al., 2014), which may result in faster growth and more carbon sequestration. Even in the work presented here, which utilized a small diatom that is not known to be a carbon-limited in current day conditions, OA still influenced aggregate formation. This is important as it helps elucidate how the biological carbon pump may be affected in ways other than changes in growth or carbon fixation, but rather on how organic molecules behave in different conditions.

Most notably, marine snow was affected by both the presence of oil compounds and by OA. Of the exudates measured, none were significantly different between the two pCO_2 levels, but instead were influenced by oil. Intracellular responses to oil conditions did not significantly change in OA, which aligns with work from others that *T. pseudonana* may have a limited response to changing carbonate conditions. This in turn shows that *T. pseudonana* is a useful species to examine because the experiment focused more on the effect of different carbonate conditions on aggregate formation than on growth conditions. The cell accumulation within aggregates was similar between the stationary and exponential growth phase experiments, but the pre-existing presence of exudates from the culture were what most likely affected the distinctive aggregate formations.

Proper response to oil spills requires knowledge of where the oil is going to travel, how it can be naturally dispersed or degraded, and the implications of using chemical dispersants. Biological events, such as MOSSFA, can significantly contribute to the sedimentation and distribution of oil (Daly et al., 2016). Modelling the impact of marine snow in oil spill conditions has been a continued effort post-DwH, and understanding how these responses may change in future ocean conditions is vital. While single strain studies are important for understanding mechanisms and the potential for change, they can also produce generalizations and oversimplifications about the effects to the ocean. Here, OA enhanced the accumulation of organic material into larger aggregates, which hypothetically would increase the sinking rates and carbon flux. However, these larger aggregates may degrade faster or get broken apart more easily in naturally turbulent conditions, which is impossible to examine in this experimental design. Exudate production may be affected by the increased availability of inorganic carbon to some phytoplankton species, and by what species are abundant within that region. Our understanding of marine oil spills and the role of phytoplankton will be further strengthened by including ocean carbonate chemistry. The results of this experiment aid towards the greater understanding of how aggregates form in OA conditions, on marine snow and MOSSFA, and the intricacies of exudates.

REFERENCES

Abbriano, R. M., Carranza, M. M., Hogle, S. L., Levin, R. A., Netburn, A. N., Seto, K. L., Snyder, S. M., and P. J. S. Franks. 2011. SIO280. Deepwater Horizon oil spill: A review of the planktonic response. Oceanography 24, 294-301.

Ambrust, E. V., Berges, J. A., Bowler, C., Green, B. R., Martinez, D., Putnam, N. H., Zhou, S., Allen, A. E., Apt, K. E., Bechner, M., Brzezinski, M. A., Chaal, B.K., Chiovitti, A., Davis, A. K., Demarest, M. S., Detter, J. C., Glavina, T., Goodstein, D., Hadi, M. Z., Hellsten, U., Hildebrand, M., Jenkins, B. D., Jurka, J., Kapitonov, V. V., Kröger, N., Lau, W. W. Y., Lane, T. W., Larimer, F. W., Lippmeier, J. C., Lucas, S., Medina, M., Montsant, A., Obornik, M., Parker, M. S., Palenik, B., Pazour, G. J., Richardson, P. M., Rynearson, T. A., Saito, M. A., Schwartz, D. C., Thamatrakoln, K., Valentin, K., Vardi, A., Wilkerson, F. P., and D. S. Rokhsar. 2004. The genome of the diatom Thalassiosira pseudonana: Ecology, Evolution, and Metabolism. Science 306, 79-86.

Arar, E., and G. Collins. 1997. In vitro determination of chlorophyll a and pheophytin a in marine and freshwater algae by fluorescence. National Exposure Research Laboratory, Office of Research and Development, US Environmental Protection Agency Method.

Aurand D., and G. Coelho. 2005. Cooperative Aquatic Toxicity Testing of Dispersed Oil and the Chemical Response to Oil Spills: Ecological Effects Research Forum (CROSERF) Lusby M.D., editor. Ecosystem Management and Associates Inc., Technical Report 07-03.

Bach, L. T., Riebesell, U., and K. G. Schulz. 2011. Distinguishing between the effects of ocean acidification and ocean carbonation in the coccolithophore Emiliania huxleyi. Limnology and Oceanography 56, 2040-2050.

Bælum, J., Borglin, S., Chakraborty, R., Fortney, J. L., Lamendella R., Mason, O. U., Auer, M., Zemla, M., Bill, M., Conrad, M. E., Malfatti, S. A., Tringe, S.G., Holman, H. Y., Hazen, T. C., and J. K. Jansson. 2012. Deep-sea bacteria enriched by oil and dispersant from the Deepwater Horizon spill. Environmental Microbiology 9, 2405-2416.

Barton, A.D., Irwin, A.J., Finkel, Z.V., and C. A. Stock. 2016. Anthropogenic climate change drives shift and shuffle in North Atlantic phytoplankton communities. Proceedings of the National Academy of Sciences 113, 2964-2969.

Basu, S., and K. R. M. Mackey. 2018. Phytoplankton as key mediators of the biological carbon pump: their responses to a changing climate. Sustainability 10(3), 869

Beardall, J., and J. A. Raven. 2013. Calcification and ocean acidification: new insights from the coccolithophore Emiliania huxleyi. New Phytologist 199, 1-3.

Behrenfeld, M. J., O'Malley, R. T., Siegel, D. A., McClain, C. R., Sarmiento, J. L., Feldman, G. C., Milligan, A. J., Falkowski, P. G., Letelier, R. M., and E. S. Boss. 2006. Climate-driven trends in contemporary ocean productivity. Nature 444, 752-755.

Bejarano, A. C., Clark, J. R., and G. M. Coelho. 2014. Issues and challenges with oil toxicity data and implications for their use in decision making: A quantitative review. Environmental Toxicology and Chemistry 33, 732-742.

Berges, J. A., Franklin, D. J., and P. J. Harrison. 2001. Evolution of an artificial seawater medium: improvements in enriched seawater, artificial water over the last two decades. Journal of Phycology 37, 1138-1145.

Bopp, L., Aumont, O., Cadule, P., Alvain, S., and M. Gehlen. 2005. Response of diatoms distribution to global warming and potential implications: A global model study. Geophysical Research Letters 32, L19606.

Bretherton, L., Williams, A. K., Genzer, J., Hillhouse, J., Kamalanathan, M., Finkel, Z. V., and Quigg, A. 2018. Physiological response of 10 phytoplankton species exposed to Macondo oil and Corexit. Journal of Phycology 54, 317-328.

Caldeira, K., and M. E. Wickett. 2003. Anthropogenic carbon and ocean pH. Nature Publishing Group 425, 365.

Chavez, F. P., Messie, M., and J. T. Pennington. 2011. Marine primary production in relation to climate variability and change. Annual Review of Marine Science 3, 227-260.

Chisholm, S. W., 2000. Oceanography: Stirring times in the Southern Ocean, Nature 407, 685-687. doi:10.1038/35037696

Chiu, M.-H., Vazquez, C. I., Shiu, R.-F., Le, C.,Sanchez, N. R., Kagiri, A., Garcia, C. A., Nguyen, C. H., Tsai, S.-M., Zhang, S., Xu, C., Santschi, P. H., Quigg, A., and W.-C. Chin. 2019. Impact of exposure of crude oil and dispersant (Corexit) on aggregation of extracellular polymeric substances. Science of the Total Environment 657, 1535-1542.

Cisternas-Novoa, C., Lee, C., and A. Engel. 2015. Transparent exopolymer particles (TEP) and Coomassie stainable particles (CSP): Differences between their origin and vertical distributions in the ocean. Marine Chemistry 1755, 56-71.

Crawfurd, K. J., Raven, J. A., Wheeler, G. L., Baxter, E. J., and I. Joint. 2011. The response on Thalassiosira pseudonana to Long-Term Exposure to Increased CO2 and Decreased pH. PLoS ONE 6 (10), e26695.

Crone, T. J., and M. Tolstoy. 2010. Magnitude of the 2010 Gulf of Mexico oil leak. Science 330, 634.

Culver, M. E., and W. O. Smith, Jr. 1989. Effects of environmental variation in sinking rates of marine phytoplankton. Journal of Phycology 25, 262–270.

Daly, K. L., Passow, U., Chanton, J., Hollander, D., 2016. Assessing the impacts of oil-associated marine snow formation and sedimentation during and after the Deepwater Horizon oil spill. Anthropocene 13, 18-33. doi:10.1016/j.ancene.2016.01.006

Finkel, Z. V., Beardall, J., Flynn, K. J., Quigg, A., Rees, T. A. V., and J. A. Raven. 2009. Phytoplankton in a changing world: cell size and elemental stoichiometry. Journal of Plankton Research 32, 119-137.

Fischer, G. and G. Karakas. 2009. Sinking rates and ballast composition of particles in the Atlantic Ocean: implications for the organic carbon fluxes to the deep ocean. Biogeosciences 6, 85-102.

Gattuso, J.-P. and H. Lavigne. 2009. Technical Note: Approaches and software tools to investigate the impact of ocean acidification, Biogeosciences 6, 2121-2133.

Gattuso, J.-P. and L. Hansson. 2011. Ocean Acidification. Oxford University Press Inc, New York.

Guillard, R. R. L. 1975. Culture of phytoplankton for feeding marine invertebrates. In Smith, W.L. and Chanley, M.H. (Eds) Culture of Marine Invertebrate Animals, Plenum Press, New York. 26-60.

Guillard, R. R. L. and J. H. Ryther, 1962. Studies of marine planktonic diatoms: I. Cyclotella nana Hustedt and Detonula confervacea Cleve Gran. Canadian Journal of Microbiology 8, 229-239.

Hung, C. C. and P. H. Santschi. 2001. Spectrophotometric determination of total uronic acids in seawater using cation exchange separation and preconcentration by lyophilization. Analytica Chimica Acta 427, 111-117.

Khatiwala, S., Tanhua, T., Fletcher, S. M., Gerber, M., Doney, S. C., Graven, H. D., Gruber, N., McKinley, G. A., Murata, A., Rios, A. F., and C. L. Sabine. 2013. Global ocean storage of anthropogenic carbon. Biogeosciences, 10, 2169-2191.

Khelifa, A., Stoffyn-Egli, P., Hill, P. S., and K. Lee. 2005. Effects of salinity and clay type on oil-mineral aggregation. Marine Environmental Research 59, 235-254.

Kolber, Z. S., Prasil, O., and P. G. Falkowski. 1998. Measurements of variable chlorophyll fluorescence using fast repetition rate techniques: defining methodology and experimental protocols. Biochimica et Biophysica Acta 1367 (1-3), 88-106.

Kromkamp, J. C., and R. M. Forster. 2003. The use of variable fluorescence measurements in aquatic ecosystems: differences between multiple and single turnover measuring protocols and suggested terminology. European Journal of Phycology 38, 103-112.

Kujawinski, E.B., Kido Soule, M.C., Valentine, D.L., Boysen, A.K., Longnecker, K., and M. C. Redmond. 2011. Fate of dispersants associated with the Deepwater Horizon oil spill. Environmental Science & Technology 45, 1298-1306. doi:10.1021/es103838p

Li, W., Gao,K., and J. Beardall. 2012. Interactive effects of ocean acidification and nitrogen-limitation on the diatom Phaeodactylum tricornutum. PLOS ONE 7, e51590, doi:10.1371/journal.pone.0051590

Mari, X. 2008. Does ocean acidification induce an upward flux of marine aggregates? Biogeosciences 5, 1023-1031.

Mari, X., Passow, U., Migon, C., Burd, A. B., and L. Legendre. 2017. Transparent exopolymer particles: Effects on carbon cycling in the ocean. Progress in Oceanography 151, 13-37. doi: 10.1016/j.pocean.2016.11.002

Mann, D. G. 1999. The species concept in diatoms. Phycologia 38, 437-495.

McCarthy, A., S. P. Rogers, S. J. Duffy, and D. A. Campbell. 2012. Elevated carbon dioxide differentially alters the photophysiology of Thalassiosira pseudonana (Bacillariophyceae) and Emiliania huxleyi (Haptophyta). Journal of Phycology 48, 635-646.

Meador, J. P. 2003. Bioaccumulation of PAHs in marine invertebrates, in PAHs: An Ecotoxicological Perspective, Douben, P. E. T., Ed., John Wiley & Sons, New York, pp. 147–171.

Milligan, A. J., D. E. Varela, M. A. Brzezinski, and F. M. M. Morel. 2004. Dynamics of silicon metabolism and silicon isotope discrimination in marine diatom as a function of pCO2. Limnology and Oceanography 49, 322-329.

Morales-McDevitt, M. E., Shi, D., Knap, A. H., Quigg, A. Sweet, S. T., Sericano, J. L., and T. L. Wade. 2019. Fate and transport of petroleum hydrocarbons in controlled mesocosm studies. In prep.

Morán, X. A. G., Lopez-Urrutia, A., Calvo-Diaz, A., and W. K. W. Li. 2010. Increasing importance of small phytoplankton in a warmer ocean. Global Change Biology 16, 1137-1144.

Morris, D. L. 1948. Quantitative Determination of Carbohydrates with Dreywood's Anthrone Reagent. Science 107, 254-5.

NOAA 2017, Mauna Loa Observatory.

Parsons, M. L., Morrison, W., Rabalais, N. N., Turner, R. E., and K. N. Tyre. 2015. Phytoplankton and the Macondo oil spill: A comparison of the 2010 phytoplankton assemblage to baseline conditions on the Louisiana shelf. Environmental Pollution 207, 152-160.

Passow, U., Alldredge, A. L., and B. E. Logan. 1994. The role of particulate carbohydrate exudates in the flocculation of diatom blooms. Deep Sea Research Part I: Oceanographic Research Papers 41, 335-357.

Passow, U., and A. Alldredge. 1995. A dye-binding assay for the spectrophotometric measurement of transparent exopolymer particles (TEP). Limnology and Oceanography 40 (7), 1326-1335.

Passow, U. 2002. Production of transparent exopolymer particles (TEP) by phyto- and bacterioplankton. Marine Ecology Progress Series 236, 1-12.

Passow, U., and C. Carlson. 2012. The Biological Pump in a High CO2 World. Marine Ecology Progress Series 470, 249–271.

Passow, U., Ziervogel, K., Asper, V., and A. Diercks. 2012. Marine snow formation in the aftermath of the Deepwater Horizon oil spill in the Gulf of Mexico. Environmental Research Letters 7, 035301.

Passow, U. 2016. Formation of rapidly-sinking, oil-associated marine snow. Deep Sea Research II: Topical Studies in Oceanography 129, 232-240.

Passow, U., and R. D. Hetland. 2016. What happened to all of the oil? Oceanography 29, 88-95.

Passow, U., and K. Ziervogel. 2016. Marine snow sedimented oil released during the Deepwater Horizon spill. Oceanography 29 (3), 118–125

Passow, U., Sweet, J., and A. Quigg. 2017. How the dispersant Corexit impacts the formation of sinking marine oil snow. Marine Pollution Bulletin 125 (1-2), 139-145.

Pedersen, M. F. and P. J. Hansen. 2003. Effects of high pH on a natural marine planktonic community. Marine Ecology Progress Series 260, 19-31.

Perry, D. M., Redman, D. H., Widman Jr., J. C., Meseck, S., King, A., and J. J. Pereira. 2015. Effect of ocean acidification on growth and otolith condition of juvenile scup, Stenotomus chrysops. Ecology and Evolution 5 (18), 4187-4196.

Pierrot, D., E. Lewis, and D. W. R. Wallace. 2006. MS Excel Program Developed for CO2 System Calculations. ORNL/CDIAC-105a. Carbon Dioxide Information Analysis Center, Oak Ridge National Laboratory, U.S. Department of Energy, Oak Ridge, Tennessee. doi: 10.3334/CDIAC/otg.CO2SYS_XLS_CDIAC105a

Ploug, H., Terbrüggen, A., Kaufmann, A., Wolf-Gladrow, D., and U. Passow. 2010. A novel method to measure particle sinking velocity in vitro, and its comparison to three other in vitro methods. Limnology and Oceanography: Methods 8, 386-393.

Quigg, A., Passow, U., Chin, W.-C., Xu, C., Doyle, S., Bretherton, L., Kamalanathan, M., Williams, A.K., Sylvan, J.B., Finkel, Z. V., Knap, A.H., Schwehr, K.A., Zhang, S., Sun, L., Wade, T.L., Obeid, W., Hatcher, P.G., and P. H. Santschi. 2016. The role of microbial exopolymers in determining the fate of oil and chemical dispersants in the ocean. Limnology and Oceanography Letters 1 (1), 3–26. doi:10.1002/lol2.10030

Quigg, A., Passow, U., Daly, K. L., Burd, A., Hollander, D. J., Schwing, P. T., and Lee, K. 2019. Chapter 12: Marine Oil Snow Sedimentation and Flocculent Accumulation (MOSSFA) events: learning from the past to predict the future. pp: 199-224, In: Murawski SA, Ainsworth C, Gilbert S, Hollander D, Paris CB, Schlüter M, Wetzel D (Eds.) Deep Oil Spills – Facts, Fate and Effects. Springer 608 pp. ISBN 978-3-030-11605-7 (eBook) https://doi.org/10.1007/978-3-030-11605-7

Reddy, C. M., Arey, J. S., Seewald, J. S., Sylva, S. P., Lemkau, K. L., Nelson, R. K., Carmichael, C. A., Mcintyre, C. P., Fenwick, J., Ventura, G. T., Van Mooy, B. A. S., and R. Camilli. 2012. Composition and fate of gas and oil released to the water column during the Deepwater Horizon oil spill. Proceedings of the National Academy of Sciences 109, 20229–20234. doi:10.1073/pnas.1101242108

Royal Society, Ocean Acidification Due to Increasing Atmospheric Carbon Dioxide, Royal Society, London, UK, 2005.

Sabine, C. L., Feely, R. A., Gruber, N., Key, R. M., Lee, K., Bullister, J. L., Wanninkhof, R., Wong, C. S., Wallace, D. W. R., Tilbrook, B., Millero, F. J., Peng, T. H., Kozyr, A., Ono, T., and A. F. Rios. 2004. The Oceanic Sink for Anthropogenic CO2. Science 305, 367.

Sammarco, P. W., Kolian, S. R., Warby, R. A. F., Bouldin, J. L., Subra, W. A., and S. A. Porter. 2013. Distribution and concentrations of petroleum hydrocarbons associated with the BP/Deepwater Horizon Oil Spill, Gulf of Mexico. Marine Pollution Bulletin 73, 129-143.

Santschi, P. H. 2018. Marine colloids, agents of the self-cleansing capacity of aquatic systems: Historical perspective and new discoveries. Marine Chemistry 207, 124-135.

Schwehr, K. A., Xu, C., Chiu, M.-H., Shang, S., Sun, L., Lin, P., Beaver, M., Jackson, C., Agueda, O., Chin, W.-C., Quigg, A., and P. H. Santschi. 2018. Protein: Polysaccharide ratio in exopolymeric substances controlling the surface tension of seawater in the presence or absence of surrogate Macondo oil with and without Corexit. Marine Chemistry 206, 84-92.

Seebah, S., Fairfield, C., Ullrich, M. S., and U. Passow. 2014. Aggregation and Sedimentation of Thalassiosira weissflogii (diatom) in a Warmer and More Acidified Future Ocean. PLoS ONE 9(11): e112379. doi:10.1371/journal.pone.0112379

Shi, Q., Xiahou, W., and H. Wu. 2016. Photosynthetic responses of the marine diatom Thalassiosira pseudonana to CO2-induced seawater acidification. Hydrobiologia 799, 361-369.

Smetacek, V. S. 1985. Role of sinking in diatom life-history cycles: ecological, evolutionary and geological significance. Marine Biology 84, 239-251.

The Federal Interagency Solutions Group (TFISG). 2010. Oil Budget Calculator Science and Engineering Team. Oil Budget Calculator Deepwater Horizon.

The chaos of clean up (TCCP). 2011. Analysis of Potential Health and Environmental impacts of chemicals in dispersant materials. (Rep Toxipedia Consulting Services and Earthjustice).

Thornton, D. C. O. 2002. Diatom aggregation in the sea: mechanisms and ecological implications. European Journal of Phycology 37, 149-161. doi: 10.1017/S0967026202003657

Thornton, D. C. O. 2009. Effect of low pH on carbohydrate production by a marine planktonic diatom (Chaetoceros muelleri). Research Letters in Ecology, Article ID 105901, doi:10.1155/2009/105901

Tortell, P. D., Payne, C. D., Li, Y., Trimborn, S., Rost, B., Smith, W. O., Riesselman, C., Dunbar, R. B., Sedwick, P., and G. R. DiTullio. 2008. CO2 sensitivity of Southern Ocean phytoplankton. Geophysical Research Letters 35 (4), doi.org/10.1029/2007GL032583

Tre´guer, P., Nelson, D. M., van Bennekom, J. V., DeMaster, D. J., Leynaert, A., and B. Que´guiner. 1995. The silica balance in the world Ocean: a reestimate. Science 268, 375-379.

Valentine, D. L., Fisher, G. B., Bagby, S. C., Nelson, R. K., Reddy, C. M., Sylva, S. P., and M. A. Woo. 2014. Fallout plume of submerged oil from Deepwater Horizon. Proceedings of the National Academy of Sciences of the United States of America 111 (45), 15906-15911.

Wade, T. L., Sweet, S. T., Sericano, J. L., Guinasso, N., Jr., Diercks, A.-R., Highsmith, R. C., Asper, V. L., Joung, D., Shiller, A. M., Lohrenz, S. E., Joye, S. B. 2011. Analyses of Water Samples from the Deepwater Horizon Oil Spill: Documentation of the Sub-Surface Plume in Monitoring and Modeling the Deepwater Horizon Oil Spill: A Record-Breaking Enterprise. AGU 195, 77–82. Geophysical Monograph Series.

Wade, T., Morales-McDevitt, M., Bera, G., Shi, D., Sweet, S., Wang, B., Gold-Bouchot, G., Quigg, A., and A. H. Knap. 2017. A method for the production of large volumes of WAF and CEWAF for dosing mesocosms to understand marine oil snow formation. Heliyon 3, e00419.

Waldbusser, G. G., Hales, B., Langdon, C. J., Haley, B. A., Schrader, P., Brunner, E. L., Gray, M. W., Miller, C. A., Gimenez, R., and G. Hutchinson. 2015. Ocean acidification has multiple modes of action on bivalve larvae. PLoS ONE 10(6): e0128376. doi:10.1371/journal.pone.0128376

Weisburd, R. S. J., Ishii, M., Fukushima, T., and A. Otsuki. 1995. Methods for measurement of dissolved inorganic carbon in natural waters Japanese Journal of Limnology 56 (3), 221-226.

Williamson, B. J., Valery U., Purvis, O. W., and B. Spiro. 2003. Characterization of airborne particulates in the Cu smelter and former mining town of Karabash, South Ural Mountains of Russia. Environmental Monitoring and Assessment 98, 235–259

Wu, Y., Campbell, D. A., Irwin, A. J., Suggett, D. J., and Z. V. Finkel. 2014. Ocean acidification enhances the growth rate of large diatoms. Limnology and Oceanography 59, 1027-1034.

Xu, C., Zhang, S., Beaver, M., Wozniak, A., Obeid, W., Lin, Y., Wade, T. L., Schwehr, K. A., Lin, P., Sun, L., Hatcher, P. G., Chin, W.-C., Chiu, M.-H., Knap, A. H., Dean, K., Quigg, A., and P. H. Santschi. 2018a. Decreased sedimentation efficiency of petro- and non-petro-carbon caused by a dispersant for Macondo surrogate oil in a mesocosm simulating a coastal microbial community. Marine Chemistry 206, 34-43. DOI: 10.1016/j.marchem.2018.09.002

Xu, C., Zhang, S., Beaver, M., Lin, P., Sun, L., Doyle, S. M., Sylvan, J. B., Wozniak, A., Hatcher, P. G., Kaiser, K., Yan, G., Schwehr, K. A., Lin, Y., Wade, T. L., Chin, W.-C., Chiu, M.-H., Quigg, A., and P. H. Santschi. 2018b. The role of microbially-mediated exopolymeric substances (EPS) in regulating Macondo oil transport in a mesocosm experiment. Marine Chemistry 206, 52-61.

Yamamoto-Kawai, M., F. A. McLaughlin, E. C. Carmack, S. Nishino, and K. Shimada. 2009. Aragonite Undersaturation in the Arctic Ocean: Effects of Ocean Acidification and Sea Ice Melt, Science 326, 1098-1100.

Yan, B., Passow, U., Chanton, J. P., Nöthig, E.-M., Asper, V., Sweet, J., Pitiranggon, M., Diercks, A., and D. Pak. 2016. Sustained deposition of contaminants from the Deepwater Horizon spill. Proceedings of the National Academy of Sciences of the United States of America 113 (24), E3332-E3340.

Yang, G., and K. Gao. 2012. Physiological responses of the marine diatom Thalassiosira pseudonana to increased pCO2 and seawater acidity. Marine Environmental Research 79, 142-151.

Yuan, W., Gao, G., Shi, Q., Xu, A., and H. Wu. 2018. Combined effects of ocean acidification and warming on physiological response of the diatom Thalassiosira pseudonana to light challenges. Marine Environmental Research 135, 63-69.

Zhang, S., Jiang, Y., Chen, C.-S., Creeley, D., Schwehr, K. A., Quigg, A., Chin, W.-C., and P. H. Santschi. 2012. Ameliorating effects of extracellular polymeric substances excreted by Thalassiosira pseudonana on algal toxicity of CdSe quantum dots. Aquatic Toxicology 126, 214-223.

APPENDIX

PAH Analysis

The PAH analysis separated the samples into compounds. For the above results sections, all PAH compounds were combined for total concentration. Here, the fingerprint of each ending time point is presented. The Naphthalene's were the most concentrated in WAF and OAWAF. DCEWAF and OADCEWAF were more dilute and had a distributed concentration of compounds.

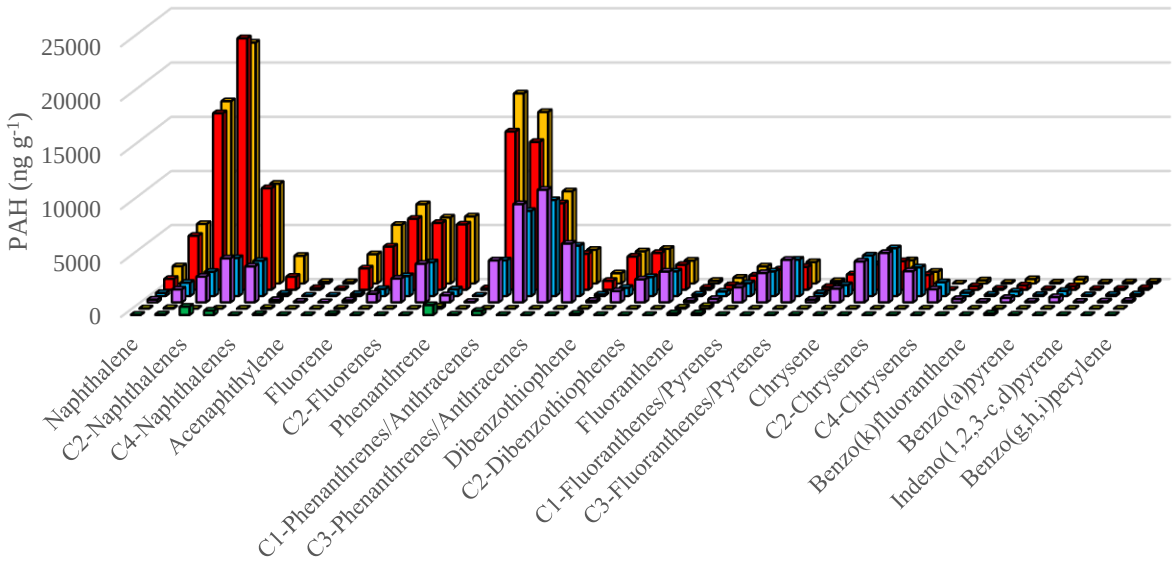

Figure A1 The final time point AGG measurements of PAH compound compounds (ng g^{-1}) in Control (green), OA (yellow), WAF (red), OAWAF (orange), DCEWAF (purple), and OADCEWAF (blue).

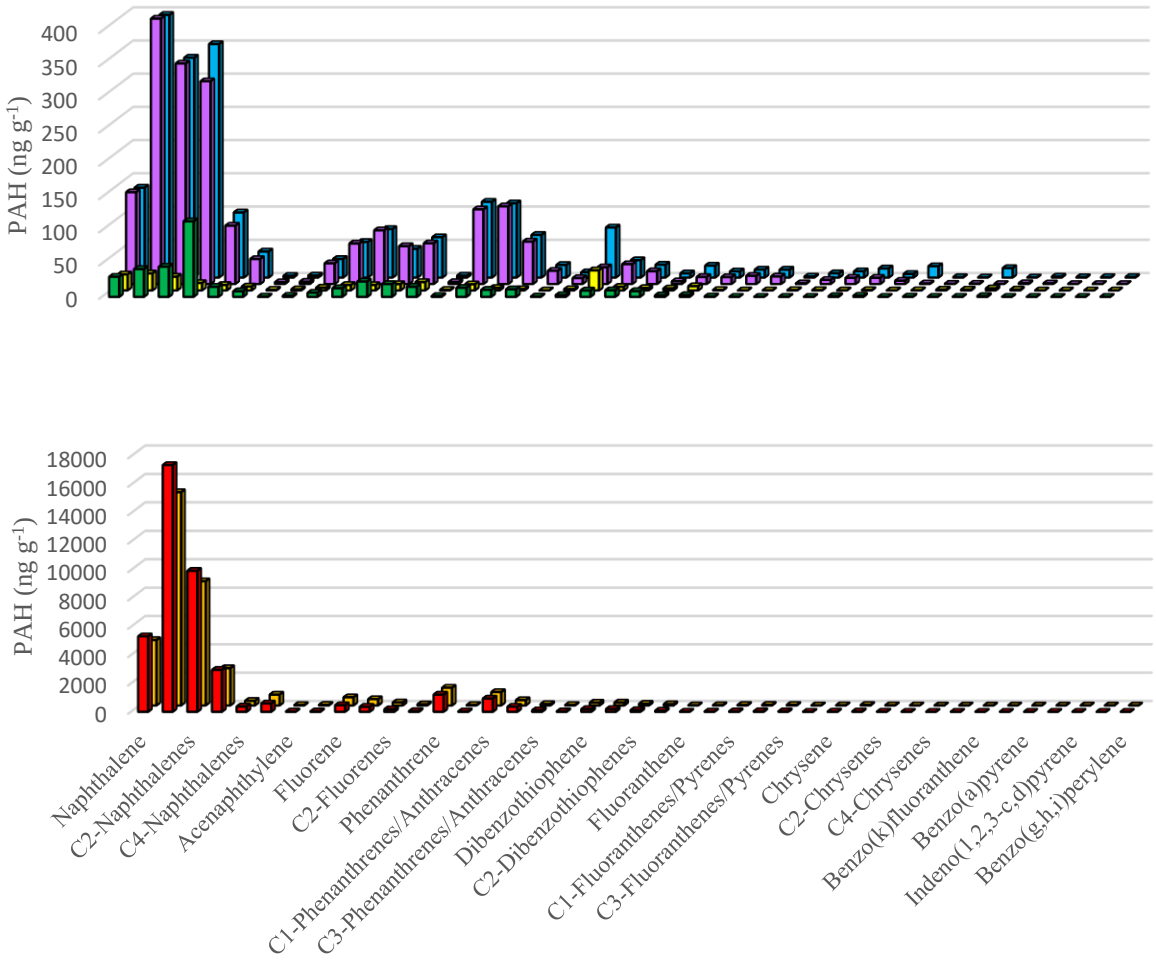

Figure A2 The final time point SSW measurements of PAH compound compounds (ng g^{-1}) in Control (green), OA (yellow), WAF (red), OAWAF (orange), DCEWAF (purple), and OADCEWAF (blue).

Artificial Seawater Recipe

This was the recipe used to make artificial seawater. Two separate solutions were made for the anhydrous and hydrated salts. First, the anhydrous salts were weighed in aluminum foil boats and individually added through a funnel into 10 L of deionized (DI) water. The funnel was rinsed with DI water between chemical additions into the carboy. Once all were added, the volume was topped off to 15 L and allowed to stir for 1 hour. The hydrated salts were added to 1 L of DI water in the same method, and the final volume was increased to 2 L for stirring. Starting with a lower volume allows for DI rinsing of the funnel between chemicals to ensure all were added. After both solutions stirred for an hour, the hydrated salt solution was added to the anhydrous. The final volume was increased to 20 L, and the combined artificial seawater was again stirred for one hour. The salinity was checked to ensure the process was successful and that the salts did not interact and precipitate out of solution.

Table A1 Artificial seawater recipe used in this study.

Component	In 1L (g)	In 20L (g)	Molar Concentration in Final Medium
Salt solution I *Anhydrous salts*			
NaCl	21.194	423.88	3.63×10^{-1} M
Na_2SO_4	3.55	71	2.50×10^{-2} M
KCl	0.599	11.98	8.03×10^{-3} M
$NaHCO_3$	0.174	3.48	2.07×10^{-3} M
KBr	0.0863	1.726	7.25×10^{-4} M
H_3BO_3	0.023	0.46	3.72×10^{-4} M
NaF	0.0028	0.056	6.67×10^{-5} M
Salt solution II *Hydrated salts*			
$MgCl_2$ $6H_2O$	9.592	191.84	4.71×10^{-2} M
$CaCl_2$ $2H_2O$	1.344	26.88	9.14 x 10-3 M
$SrCl_2$ $6H_2O$	0.0218	0.436	8.18×10^{-5} M

Berges, J.A., Franklin, D.J. and Harrison, P.J. 2001. Evolution of an artificial seawater medium: improvements in enriched seawater, artificial water over the past two decades. *J. Phycol*. 37: 1138-1145.

Harrison, P.J., Waters, R.E., and Taylor, F.J.R. 1980. A broad spectrum artificial seawater medium for coastal and open ocean phytoplankton. *J. Phycol.* 16: 28-35.

Exudates

The exudate measurements compiled.

Table A2 Exudate measurements included total colloidal EPS (mg) and TEP (mg Gxan) in SSW, particulate EPS in AGG, and proteins-C to carbohydrates-C stickiness ratio in both fractions.

Treatment	Colloidal (mg)		Particulate (mg)		Protein:TCHO		TEP (mg GXan)
	SSW		AGG				
	Protein	TCHO	Protein	TCHO	Colloidal	Aggregate	SSW
Control	0.75 (± 0.15)	0.42 (± 0.08)	0.31 (± 0.06)	0.55 (± 0.23)	2.52 (± 0.74)	1.57 (± 0.13)	1.36 (± 0.08)
OA	0.61 (± 0.06)	0.41 (± 0.17)	0.27 (± 0.05)	0.50 (± 0.81)	2.40 (± 0.92)	2.16 (± 0.47)	1.20 (± 0.15)
WAF	1.01 (± 0.16)	0.60 (± 0.18)	0.13 (± 0.03)	0.27 (± 0.16)	2.39 (± 0.31)	1.18 (± 0.25)	3.86 (± 0.35)
OAWAF	1.01 (± 0.05)	0.62 (± 0.04)	0.42 (± 0.17)	0.76 (± 0.55)	2.22 (± 0.04)	2.03 (± 0.87)	3.90 (± 0.47)
DCEWAF	0.88 (± 0.17)	0.65 (± 0.18)	0.30 (± 0.06)	0.60 (± 0.28)	2.00 (± 0.76)	2.17 (± 0.11)	-
OADCEWAF	1.30 (± 0.18)	0.65 (± 0.14)	0.20 (± 0.17)	0.49 (± 0.16)	2.90 (± 0.85)	2.54 (± 0.21)	-

Optical density ImageJ Analysis

For ImageJ analysis, the photograph of a tank was first converted from color to grey scale. Using the Interactive 3d Surface Plot and the Spectrum LUT (Look Up Table) tool within the software creates a heat plot of an aggregate. This can be beneficial to visualize how the program takes the pixels within the selection and calculates a mean grey value. The scale bar is inverted here compared to the grey scale values shown in the results section. Here, two aggregates of easily distinguishable densities were selected to highlight differences.

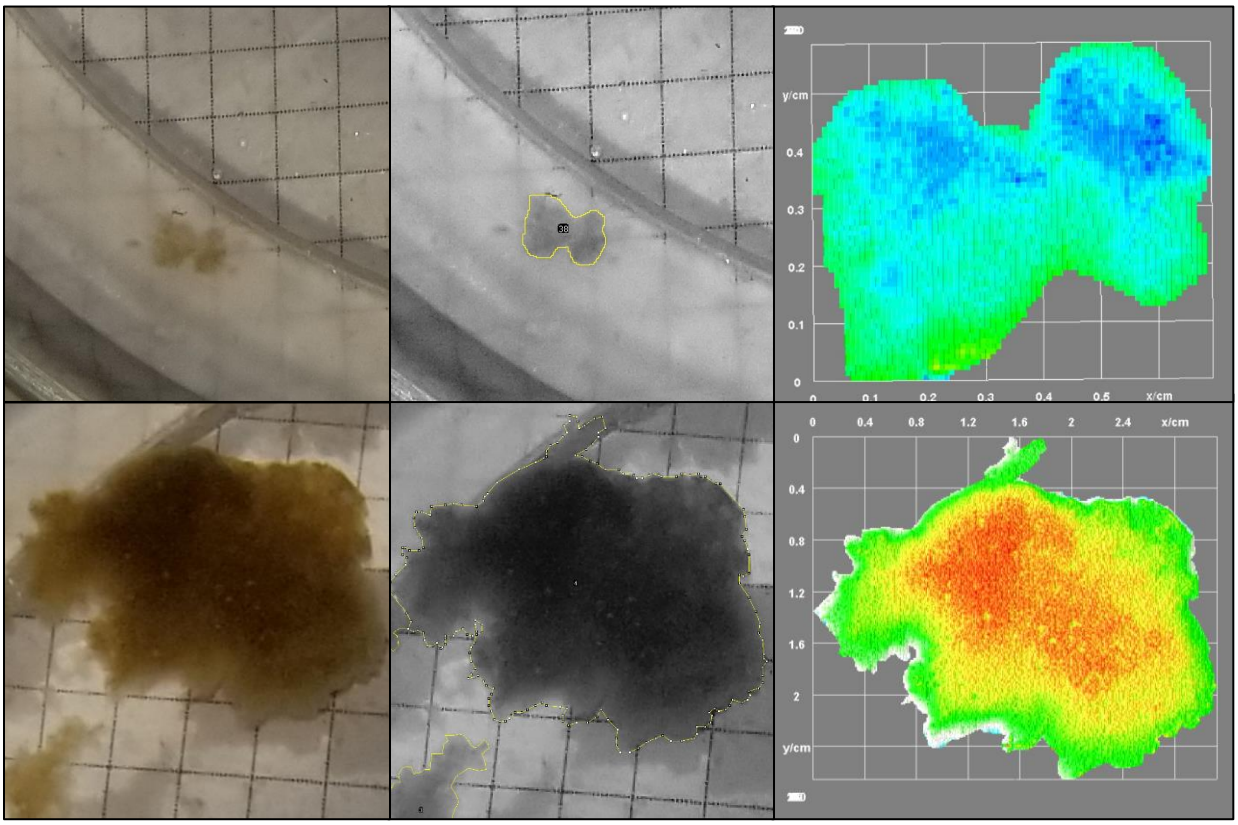

Figure A3 Two aggregates of varying density compared in color, grey scale, and with an ImageJ generated heat plot.

Exudate relationships

Average final TEP measurements were strongly correlated with all SSW EPS materials (Figure A4). In Passow et al. (2019), TEP was not significantly correlated with EDTA-extractable neutral sugars, but with EDTA-extractable uronic acids and proteins.

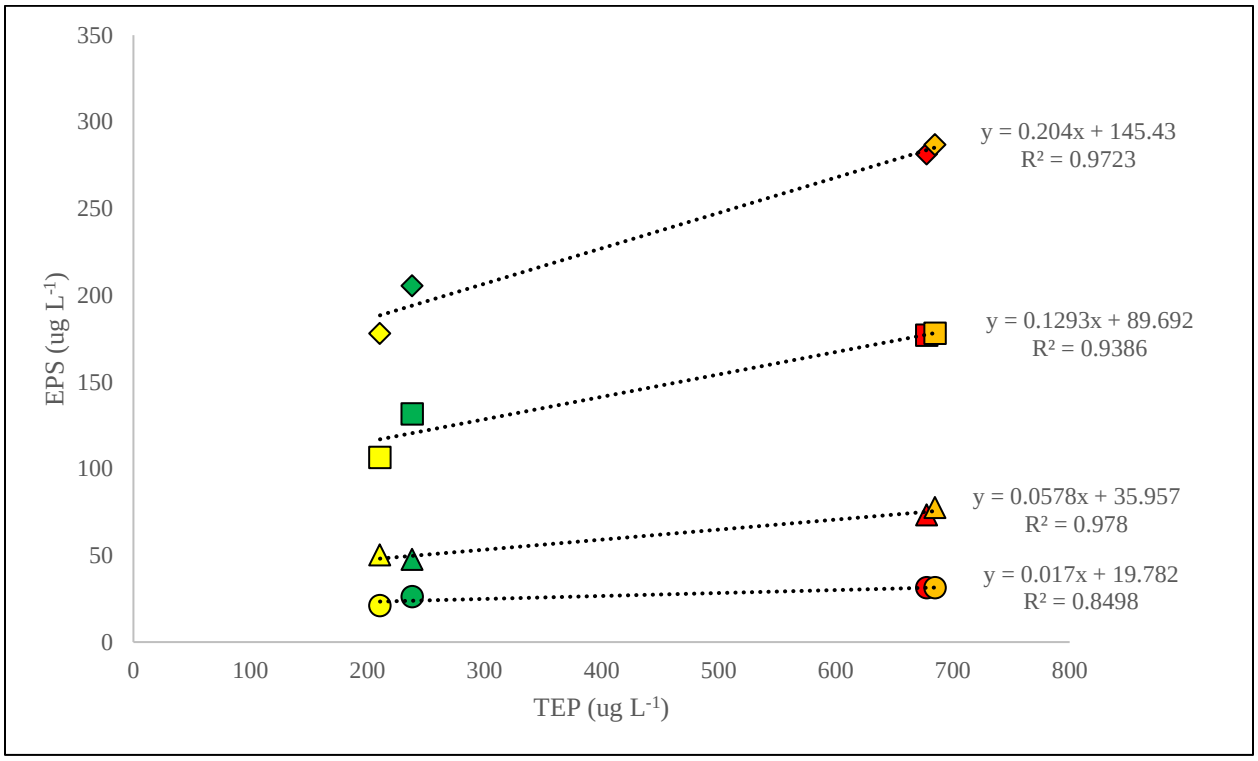

Figure A4 The final SSW EPS and TEP measurements show correlations with total EPS (diamond), proteins (square), uronic acids (circle), and neutral sugars (triangle) in Control (green), OA (yellow), WAF (red), and OAWAF (orange) treatments.

Aggregate distribution

The aggregate counts increased with the presence of oil compounds in the exponential growth phase experiment. OADCEWAF produced the most aggregates, and Controls the least.

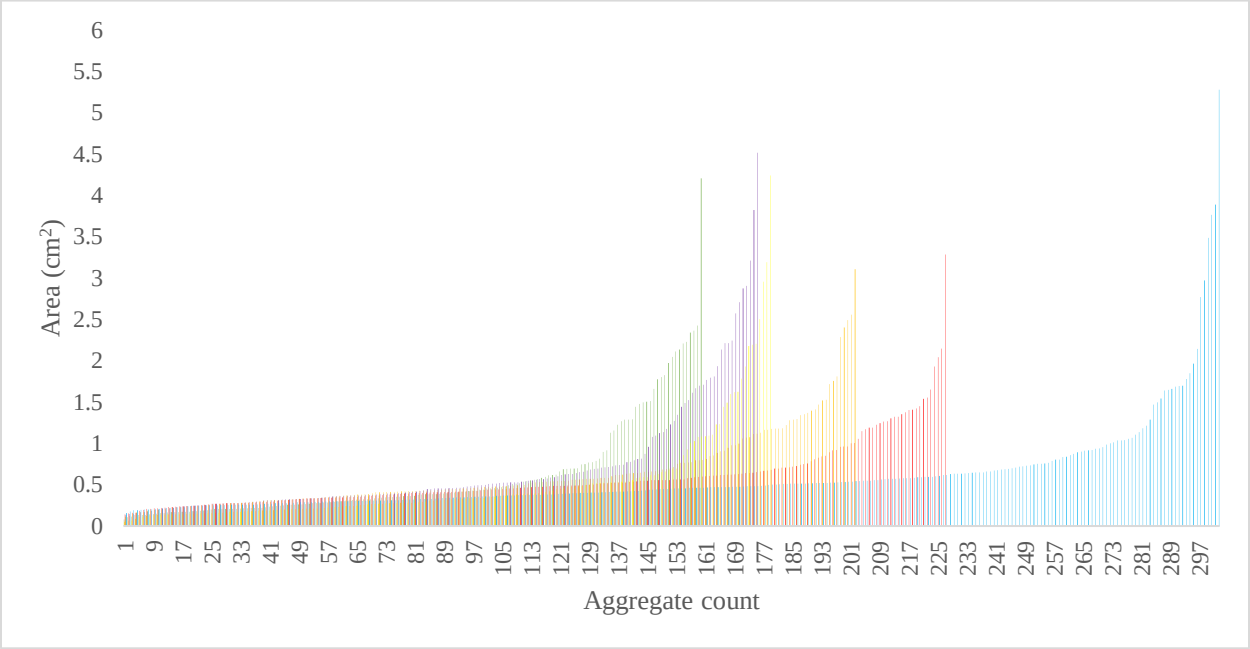

Figure A5 All replicates in the exponential growth phase experiment were combined in Control (green), OA (yellow), WAF (red), OAWAF (orange), DCEWAF (purple), and OADCEWAF (blue) to display total aggregate counts and size (cm^2) distribution.

Aggregate dendrogram

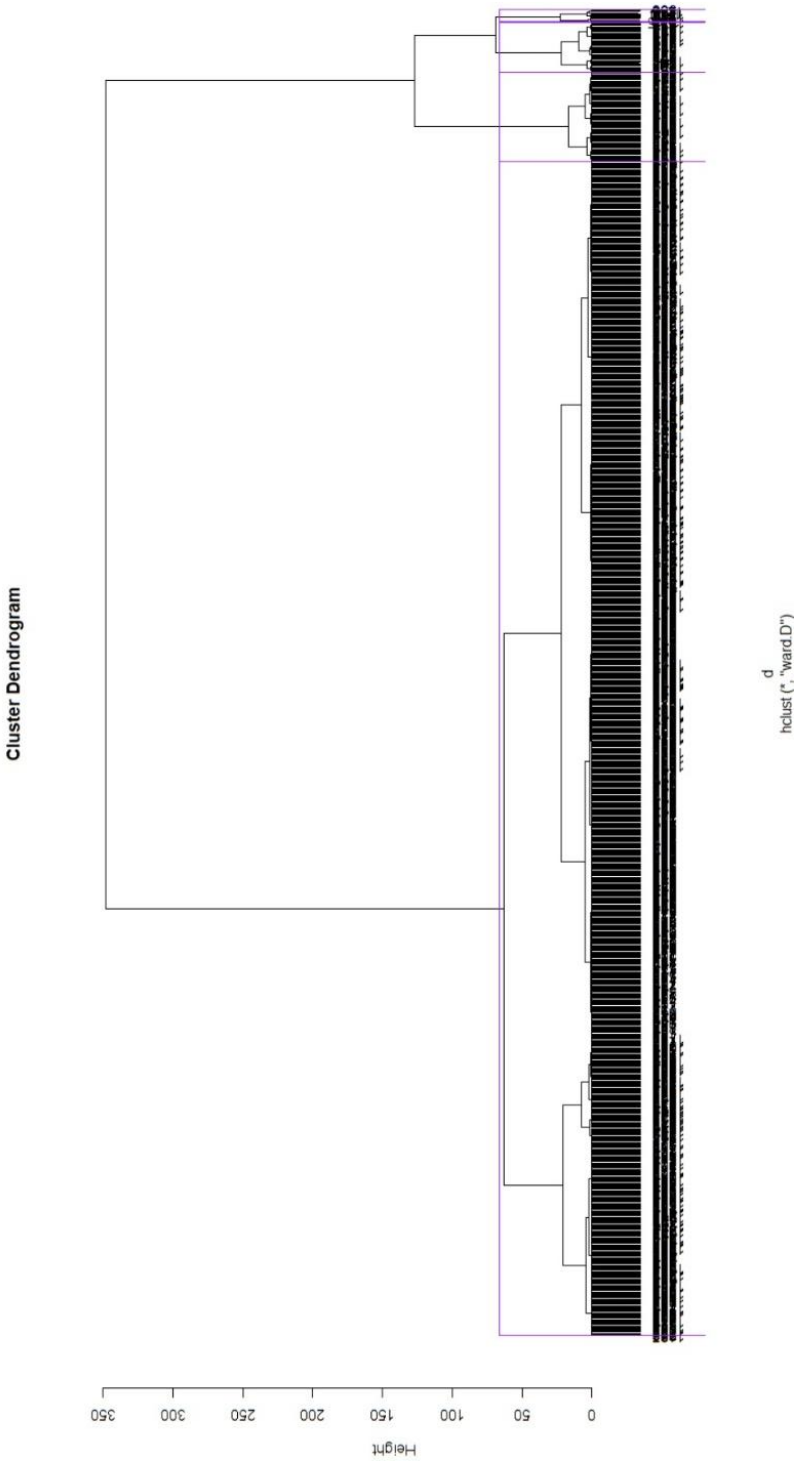

Figure A6 The cluster dendrogram built using RStudio was used to determine size classes. The purple boxes indicate the four separate size classes.